Article title:

An Aminoacyl tRNA Synthetase, OKI1, Is Required for Proper Shoot Meristem Size in *Arabidopsis*

Running title:

An aaRS OKI1 is required for proper meristem size

Corresponding author:

Dr. D. Jackson

Cold Spring Harbor Laboratory, 1 Bungtown road, Cold Spring Harbor, New York, 11724

Phone: +1-516-367-8467

Fax: +1-516-367-8369

E-mail: jacksond@cshl.edu

Subject area:

Growth and development

Black and white figures: 0

Color figures: 5

Tables: 0

Supplemental materials: 7

Title and running head:

An Aminoacyl tRNA Synthetase, OKI1, Is Required for Proper Shoot Meristem Size in *Arabidopsis*

An aaRS OKI1 is required for proper meristem size

Author names:

Munenori Kitagawa[1†], Rachappa Balkunde[1,2†], Huyen Bui[1,3] and David Jackson[1]*,

[†] These authors contributed equally to this work.

Author addresses:

[1] Cold Spring Harbor Laboratory, 1 Bungtown road, Cold Spring Harbor, New York, 11724, USA

[2] Washington University in St.Louis, 1 Brookings Drive, St. Louis, Missouri, 63130, USA

[3] School of Biological Sciences, University of Utah, 257 South 1400 East, Salt Lake City, Utah, 84112, USA

Corresponding author:

Dr. David Jackson

Cold Spring Harbor Laboratory, 1 Bungtown road, Cold Spring Harbor, New York, 11724

Phone: +1-516-367-8467

Fax: +1-516-367-8369

E-mail: jacksond@cshl.edu

Abbreviations:

aaRS	Aminoacyl tRNA synthtase
ABPH2	ABERRANT PHYLLOTAXY2
AS1	ASYMMETRIC LEAVES1
AsnRS	Asparaginyl-tRNA synthetase
AspRS	Aspartyl tRNA synthetase
BABA	β-aminobutyric acid
BAM	BARELY ANY MERISTEM
BEN1	BRI 1-5 ENHANCED 1
CAPS	cleavable amplified polymorphic sequence
CLV	CLAVATA
CRN	CORYNE
CZ	central zone
DAB	3,3'-diaminobenzidine
DAP	days after planting
dCAPS	derived cleavable amplified polymorphic sequence
DCL	DEFECTIVE CHLOROPLASTS AND LEAVES
EDD1	EMBRYO DEFECTIVE DEVELOPMENT1
EMS	ethyl methane sulfonate
FEA4	FASCIATED EAR4
GAT1	GFP ABERRANT TRAFFICKING1
GFP	green fluorescent protein
GUS	β-glucuronidase

68	HAM	HAIRY MERISTEM
69	IBI1	IMPAIRED IN BABA-INDUCED IMMUNITY1
70	LRR-RLK	leucine-rich repeat receptor like protein kinase
71	LysRS	Lysyl-tRNA synthetase
72	NBT	nitroblue tetrazolium
73	MS	Murashige and Skoog
74	MSCA1	MALE STERILE CONVERTED ANTHER1
75	mTOR	mammalian target of rapamycin
76	OB	oligonucleotide-binding
77	OC	organizing center
78	OKI1	OKINA KUKI
79	PFA	paraformaldehyde
80	PGY	PIGGYBACK
81	PI	propidium iodide
82	PHB	prohibitin
83	PZ	peripheral zone
84	RML1	RICE MINUTE-LIKE1
85	ROS	reactive oxygen species
86	SAM	shoot apical meristem
87	SerRS	Seryl-tRNA synthetase
88	SNP	single nucleotide polymorphism
89	TAC	transformation-competent artificial chromosome
90	WT	wild type

91 WUS WUSCHEL

92

Abstract

In plants, the stem cells that form the shoot system reside within the shoot apical meristem (SAM), which is regulated by feedback signaling between the WUSCHEL (WUS) homeobox protein and CLAVATA (CLV) peptides and receptors. WUS-CLV feedback signaling can be modulated by various endogenous or exogenous factors such as chromatin state, hormone signaling, reactive oxygen species (ROS) signaling and nutrition, leading to a dynamic control of SAM size corresponding to meristem activity. Despite these insights, however, the knowledge of genes that control SAM size is still limited, and in particular the regulation by ROS signaling is only beginning to be comprehended. Here, we report a new gene that functions in SAM size maintenance, *OKINA KUKI* (*OKI1*), which is expressed in the SAM and encodes a mitochondrial aspartyl tRNA synthetase (AspRS). *oki1* mutants display enlarged SAMs with abnormal expression of WUS and CLV3, and overaccumulation of ROS in the meristem. Our findings support the importance of normal AspRS function in the maintenance of the WUS-CLV3 feedback loop and SAM size.

Keywords:

Aminoacyl tRNA synthetase

Arabidopsis thaliana

Fasciation

Mitochondria

Redox

Shoot meristem

Introduction

Stem cells are responsible for the generation of new tissues and organs in multicellular organisms, while maintaining themselves as pluripotent initials. In plants, stem cells reside in meristems, and the shoot apical meristem (SAM) can generate all shoot organs, such as leaves and flowers. Semi-permanent stem cells are found at the apical region of the SAM, in the central zone (CZ), and the organizing center (OC) below is a group of niche cells that provides cues to the CZ for stem cell maintenance. The daughter cells produced by stem cell divisions are displaced to the peripheral zone (PZ), where they form organ primordia, and in turn differentiate into lateral organs. Thus, stem cell fate and differentiation are precisely regulated depending on position within the SAM, allowing maintenance of the stem cell population and meristem size.

For such position dependent maintenance of the stem cell niche, plants have developed a negative feedback signaling pathway. The homeodomain transcription factor WUSCHEL (WUS) is expressed in the OC, and moves through plasmodesmata into the CZ to activate the expression of its negative regulator CLAVATA3 (CLV3) (Daum et al. 2014; Fletcher et al. 1999; Mayer et al. 1998; Perales et al. 2016; Yadav et al. 2011). CLV3 is a secreted peptide perceived by the leucine-rich repeat receptor like protein kinases (LRR-RLKs) CLAVATA 1 (CLV1) and the related BARELY ANY MERISTEM (BAMs) as well as by the LRR receptor like protein CLAVATA2 (CLV2) in a complex with the CORYNE (CRN) pseudokinase, which together repress the expression of WUS in the OC (Clark et al. 1997; DeYoung et al. 2006; DeYoung and Clark 2008; Hu et al. 2018; Kayes and Clark 1998; Miwa et al. 2008; Muller et al. 2008; Nimchuk et al. 2011; Nimchuk et al. 2015; Ogawa et al. 2008; Shinohara and Matsubayashi 2015). This WUS-CLV3 negative feedback loop establishes a self-correcting mechanism that

maintains proper size of the stem cell pool and the meristem (Brand et al. 2000; Schoof et al. 2000; Somssich et al. 2016).

The WUS-CLV negative feedback loop is also regulated by various endogenous and exogenous signals. For example, precise WUS expression patterns require chromatin regulators, and mutants of these factors display bigger and disorganized meristems (Graf et al. 2010; Kaya et al. 2001). In addition, cytokinin promotes WUS expression and in turn facilitates the proliferation of stem cells, leading to an increase in SAM size (Chickarmane et al. 2012; Gordon et al. 2009; Gruel et al. 2016; Landrein et al. 2014). Cytokinin signaling also controls SAM size depending on the availability of nutrients in a WUS-dependent manner, allowing plants to optimize shoot organogenesis according to resource availability (Landrein et al. 2018). By contrast, auxin signaling negatively regulates the stem cell population by modulating WUS-CLV3 feedback loop through interaction with cytokinin signaling (Shi et al. 2018; Zhao et al. 2010). ROS signaling is also an important regulator of the stem cell population and SAM size. Mutants of a mitochondrial protease and plastid ion channels display abnormal accumulation of ROS at the shoot apices under abiotic stresses, leading to premature termination of the SAM and abnormal growth of calluses at the shoot apices, respectively (Dolzblasz et al. 2016; Wilson et al. 2016). Furthermore, Zeng et al. (2017) reported that superoxide anions are enriched in the stem cells of the SAM and promote WUS expression, whereas hydrogen peroxide accumulates in the PZ to promote differentiation. These findings suggest that the proper accumulation and precise distribution of ROS are crucial for the maintenance of stem cell niches and SAM size. The same applies for regulating the root apical meristem (Jiang et al. 2003; Kong et al. 2018; Tsukagoshi et al. 2010; Yang et al. 2014; Yu et al. 2016; Yu et al. 2013). For example, a recent study revealed that prohibitin (PHB3) regulates ROS homeostasis in roots, and in turn maintains root meristem

size and stem cell niches through the functions of its downstream ROS-responsible factors; *phb3* mutants show overaccumulation of ROS in roots, reduced root meristem size and defective quiescent center (Kong et al. 2018).

Despite these insights, the knowledge of genes affecting SAM size is limited, and how ROS is regulated in the SAM is only beginning to be understood. In this study, we identify the *OKINA KUKI* (*OKI1,* Japanese for big stem) gene as a new factor in SAM size maintenance. *oki1* mutant seedlings have enlarged SAMs and abnormal expansion of WUS and CLV3 expression. *OKI1* encodes a mitochondrial aspartyl-tRNA synthetase (AspRS) that is expressed in the SAM. In general, aminoacyl-tRNA synthetases (aaRSs) catalyze the addition of amino acid to their cognate tRNAs to prepare substrates for protein translation, and mitochondrial aaRSs are key components of the mitochondrial translation apparatus (Sissler et al. 2017; Vargas-Rodriguez et al. 2018). Therefore *oki1* mutation could affect mitochondrial translation and consequently mitochondrial functions (Robles and Quesada 2017). Mitochondria act as a powerhouse to produce energy for cells, and also produce ROS signals affecting various cellular functions, such as stress responses, hormone signaling and development (Huang et al. 2016). For example, in the meristem, mitochondria function in generation of ROS signals that affect meristem size and cell cycle (Schippers et al. 2016). Indeed, mutants in a rice mitochondrial and cytoplasmic aaRS display abnormal accumulation of ROS in meristematic tissues of the early anther, resulting in overproliferation and disorganization of cells (Yang et al. 2018). Our data also showed that ROS accumulates in the SAM of *oki1*, suggesting a possible mechanism for abnormal meristem development. Collectively, our discoveries suggest that normal function of the AspRS OKI1 is required to maintain the WUS-CLV3 feedback loop and SAM size.

185 **Results**

186 In an ethyl methyl sulfonate (EMS) screen for new mutants affecting shoot development
187 in *Arabidopsis*, we identified a mutant with small seedlings and the first 4-5 leaves were narrow
188 and strap shaped (Fig. 1A, B). Later in development, the plants recovered their growth somewhat,
189 and made inflorescence shoots that were often highly fasciated (54%, n= 20/37, Fig. 1D-F) with
190 asymmetrically lobed rosette leaves. As the fasciation phenotype is usually associated with
191 enlargement in meristem size (Fig. 1C), we measured shoot meristems from the mutants and
192 their normal siblings (Fig. 1G-J). The mutant meristems were normal at 8 days after planting
193 (DAP), but were significantly wider and taller than their siblings at 12 DAP ($N = 10\text{-}15$; $P < 0.01$,
194 Tukey HSD test). To understand the cellular basis of this phenotype, we fixed and sectioned both
195 shoot and root apices for imaging in the confocal microscope. Normal shoot meristems have
196 cells arranged in two regular outer layers, the L1 and L2, with an inner group of L3 cells (Fig.
197 1K, L). In contrast, the mutant shoot meristems had highly disorganized cell arrangement, and
198 the regular L1 and L2 layer structure was less evident (Fig. 1M, N). Similar phenotypes were
199 found in root meristems, where cells are again normally arranged in regular radial layers (Fig.
200 1O, P). In the mutants, we again saw evidence of irregular layers, with cells expanding into the
201 space of the adjacent layers, and irregular planes of cell division (Fig. 1Q, R). Because of the
202 prominent fasciated stem phenotype, we named this mutant *okina kuki* (*oki1*, Japanese for big
203 stem).

204 The *oki1* mutant was identified in Columbia-0 (Col-0), so to identify the underlying gene
205 we crossed it to the *Landsberg erecta* (Ler) ecotype, and made a bulk mutant pool from the F2
206 mapping population. We next used whole genome sequencing, followed by analysis using the
207 SHOREmap pipeline (Schneeberger et al. 2009) to map the mutation to chromosome 4, between

~ 15-17 Mb. Further fine mapping, combined with analysis of gene sequences within the mapping interval revealed a candidate mutation in AT4G33760, a gene encoding an aspartyl tRNA synthetase. A single base pair change, G347A, in the first exon of this gene led to a single predicted amino acid change, G116D, in the anti-codon binding domain of this protein (Fig. 2A and B). This 116th Glycine is fully conserved in plants and animals (Fig. 2C). To confirm this was the correct mutation underlying the phenotype, we obtained a putative null allele, SAIL_358_B08, with a T-DNA insertion in the 10th exon of AT4G33760 (Fig. 2A), and when plants heterozygous for this insertion were crossed to *oki1* plants, the T-DNA insertion allele failed to complement the *oki1* phenotype, as the progeny segregated ~ half with *oki1* phenotype (Fig. 2D and Fig. S1A), and these plants were confirmed as being heterozygous for the *oki1* EMS allele and the T-DNA mutations. Furthermore, we were able to complement the *oki1* mutation using a TAC clone, JAtY59F05, containing AT4G33760 (Fig. S1B), but not when AT4G33760 in this TAC was mutated by creating a frameshift by inserting a mCherry-Amp^{R} cassette in the fourth exon, together indicating that the gene underlying the *oki1* mutation was correctly identified.

Aminoacyl tRNA synthetases play a critical role in cellular metabolism by charging tRNAs with their cognate amino acid for protein synthesis. *Arabidopsis* encodes three aspartyl tRNA synthetases (Fig. 2E), and the one encoded by AT4G33760 is expressed ubiquitously, with strongest expression in seedling leaves and vegetative shoot meristems (Fig. S2). The product of AT4G33760 is predicted to localize to mitochondria and/or chloroplasts (Duchêne et al. 2005), while the two other aspartyl tRNA synthetases, At4G26870 and At4G31180 are predicted to encode cytoplasmic proteins (Fig. 2E) (Luna et al. 2014). To ask where the OKI1 protein localized, we made a triple YPet fluorescent protein fusion tagged at the C terminus of the

predicted coding sequence, in the context of its native regulatory sequences in the TAC clone. This construct was able to fully complement the mutant phenotype, and in the protoplasts prepared from mature leaf tissues, we observed OKI1-YPet localization in a punctate pattern that overlapped with a mitochondrial stain, MitoTracker Red (Fig. S3A-D). In shoot meristems, we also saw punctate staining (Fig. 3A, B), that again co-localized with MitoTracker Red, and not with plastids, visualized by autofluorescence (Fig. 3C-G). In summary, we identified *oki1* as a point mutation in an aspartyl tRNA synthetase that localizes to mitochondria in the leaf and shoot meristem, and is a weak allele, since a putative null allele SAIL_358_B08 was lethal.

We next ask how the *oki1* mutant interacted with the canonical CLV-WUS feedback pathway that maintains the stem cell population in the shoot meristem. We crossed the *oki1* mutant to a line carrying a GFP reporter for CLV3, as well as a RFP reporter for WUS expression. In wild type (WT) siblings, these reported the expected expression, with CLV3 expressed in 2 to 3 cell layers of stem cells in an arc at the top of the meristem, and WUS in a cluster of organizing center cells below in red (Fig. 4B, F). In the mutants, the separation of the CLV and WUS domains was maintained, however the meristems were enlarged and irregular, as already described, and the CLV3 and WUS expression domains were expanded (Fig. 4D, H and Fig. S4). We also asked how these mutations interact in double mutant combinations. *wus* mutants make irregular shoots that terminate prematurely, and even after bolting make few, irregular flowers (Fig. 4K, L). In double *wus oki1* mutants, *wus* behaved epistatically, as the double mutants were indistinguishable from *wus* (Fig. 4K-N). *clv3 oki1* double mutants similarly resembled the *clv3* single mutants (Fig. 4O, P), and quantification of phenotypes by measurements of stem thickness indicated that there was no significant difference in stem thickness between *oki1* or *clv3* single mutants and *oki1 clv3* double mutants (Fig.S5). Together

these double mutant analyses indicate that *wus* and *clv3* are epistatic to *oki1* in meristem size control.

Finally, to address the possible mechanism by which *oki1* mutants cause meristem disruption, we reasoned that a block in mitochondrial function by partial loss of an essential translation factor might lead to redox inbalance, which is known to impact meristem size (Zeng et al. 2017). We therefore stained meristems with redox dyes, and indeed found that superoxide and peroxide were upregulated in *oki1* meristems (Fig. 5), suggesting that redox imbalance may cause the increases in meristem size in *oki1*. Additionally, an OKI1 homolog in *Arabidopsis*, the AspRS IMPAIRED IN BABA-INDUCED IMMUNITY 1 (IBI1; AT4G31180, Fig. 2E) acts as a receptor of β-aminobutyric acid (BABA) in addition to its housekeeping function. BABA is a nonprotein amino acid that protects plants against broad-spectrum diseases (Luna et al., 2014). To ask if OKI1 is also involved in BABA signaling, we investigated the BABA sensitivity of *oki1* mutants (Fig. S6). However, *oki1* growth was normal in the presence of BABA concentrations that severely inhibit *ibi1* growth (Fig. S6B, C), suggesting that *oki1* does not function in BABA signaling.

Discussion.

Meristems are highly ordered structures that initiate new organs throughout the lifecycle, to enable plant survival. Several mutants with disorganized meristems has been described, and among the ones with larger meristems the best understood are the CLV pathway genes, *CLV1*, *CLV2* and *CLV3*, which repress *WUS* to balance the loss of cells from the meristem due to organ initiation with the production of cells by stem cell divisions. This balance is crucial to maintain meristem size, and other genes acting in the peripheral zone of the meristem, either providing feedback to the stem cell niche or promoting the transition of cells into organ primordia, also lead to bigger meristems when mutated (Chuck et al. 2014; Pautler et al. 2015). Hormonal feedback signaling, most notably by cytokinins, and chromatin level regulation of WUS expression are also important in meristem size control, and can lead to bigger meristems when disrupted (Chickarmane et al. 2012; Gordon et al. 2009; Gruel et al. 2016; Kaya et al. 2001; Landrein et al. 2014). Here we report a new mutant with large meristems, *oki1*, that encodes an aspartyl tRNA synthetase. *Arabidopsis* encodes three aspartyl tRNA synthetase homologs, with two predicted to encode cytoplasmic proteins, and OKI1 is the only to encode a protein that is predicted to be localized to organelles. We found using a functional YPet fusion that the OKI1 protein product localizes predominantly to mitochondria. Not surprisingly, a putative *oki1* null mutant SAIL_358_B08 was lethal, however we identified a viable, and therefore weak, allele uncovering a function of the *OKI1* aspartyl tRNA synthetase in meristem maintenance that could not be elucidated from null alleles.

Analysis of meristem structure in the *oki1* weak allele provided important insights into development. First, the organization of cells into regular clonal cell layers was disrupted in both

shoot and root, however the meistems were able to function and complete the plant lifecycle, including production of viable flowers and seeds. This supports the idea that plant development is controled by positional information, and even where clonal divisions are observed, such as in meristems, such regular divisions are not essential for maintaining stem cell niches (Smith et al. 1996). Moreover, we found that expression of both CLV3 and WUS genes were maintained as correctly positioned separate domains, further supporting the idea that these domains are established using positional cues rather than a dependency on cell lineage. In addition to the meristems, leaf development was also severely disrupted in *oki1* mutants; the first leaves produced were narrow and strap shaped, and later leaves were asymmetrically lobed. Therefore full *OKI1* function appears necessary for many aspects of *Arabidopsis* development.

What is the mechanism of *OKI1* function? AaRSs perform housekeeping roles in protein translation, by catalyzing the ligation of amino acids and their cognate transfer tRNAs to prepare substrates for protein translation (Vargas-Rodriguez et al. 2018). In plants, translation occurs in three different cellular compartments, the chloroplasts, mitochondria and cytosol (Berg et al. 2005). Translation in each of these compartments is necessary, as elimination of some chloroplast, mitochondria or cytosol aaRSs in *Arabidopsis* leads to embryo lethality, ovule abortion or gametophytic lethality (Berg et al. 2005). A putative null mutant in *OKI1* is also lethal, but the weak *oki1* allele is viable, with severe effects on meristem and organ growth. The *oki1* weak mutant phenotype differed from most meristem mutations, in that the cellular organization was highly irregular, and suggest that it may function through a different mechanism compared to the canonical meristem pathways. This weak allele has a single amino acid substitution in the conserved oligonucleotide-binding (OB) fold domain, which is involved

317 in recognition of the anti-codon in the mRNA by the charged tRNA (Mirande 2017). Therefore
318 this mutation is predicted to disrupt translation, presumably in mitochondria. Therefore it may
319 affect the energy balance of cells, and it is not surprising that the phenotype is evident in
320 meristems and developing primordia, where energy demand for growth is high. However, it is
321 surprising that the mutation leads to meristem enlargement, since most similar mutations do not.
322 One other developmental mutant in an organellar targeted tRNA synthetase gene, a glycyl tRNA
323 synthetase, is a weak allele of *EMBRYO DEFECTIVE DEVELOPMENT1* (*EDD1*), that is lethal
324 in null alleles (Moschopoulos et al. 2012). Weak *edd1* mutants enhance *asymmetric leaves1*
325 *(as1)* phenotypes, and affect genes involved in leaf dorsiventral polarity, though again the
326 mechanism is unknown, and no meristem phenotype was reported or is evident in *edd1* mutants.
327 Leaf development is also abnormal in *defective chloroplasts and leaves* (*dcl*) mutants in
328 *Arabidopsis* and tomato; *DCL* encodes a plastid targeted protein that functions in ribosomal
329 RNA processing, but again no effect on meristem size was reported (Bellaoui and Gruissem
330 2004; Bellaoui et al. 2003). Other mutations with developmental phenotypes affect the
331 cytoplasmic translational machinery, including ones in the *PIGGYBACK* (*PGY*) genes in
332 *Arabidopsis*; *pgy* mutants were first identified in a screen for leaf polarity mutants in
333 *Arabidopsis*, and encode ribosomal large subunit proteins (Pinon et al. 2008). Mutants in a
334 related gene also affects leaf development in rice, for example *rice minute-like1* (*rml1*) mutants
335 are smaller with defective vascular patterning and narrow leaf blades, and may have auxin
336 related defects, however again no effect on meristem size or organization were reported (Zheng
337 et al. 2016). *rml1* mutants also have small panicles, suggesting that shoot meristem size is
338 reduced, which may reflect defects in cell growth or proliferation expected when ribosomes are
339 compromised. Alternatively, it is possible that the specific developmental phenotypes of

ribosomal mutants reflects a true regulatory role in development (Byrne 2009). However all of the plant mutants affecting ribosomes or translational machinery have abmormal leaf development with no obvious defect in meristems, and no reported example of meristem enlargement or fasciation, suggesting the *oki1* phenotype is unique. One possible mechanism to explain *oki1* phenotypes is that the OKI1 protein has an additional function, distinct from its role in translation. In mammals, aaRSs have alternative functions, such as in transcriptional control, extracellular receptor-mediated signaling or in mammalian target of rapamycin (mTOR) signaling (Schimmel 2018). In *Arabidopsis*, an *OKI1* homolog, the AspRS IBI1 functions in a noncanonical way in plant defense to perceive BABA (Luna et al. 2014). BABA binds to IBI1 and blocks its L-Asparate binding site, switching the AspRS canonical activity of IBI1 to the noncanonical defense activity upon pathogen infection. However this is unlikely to be the case for *OKI1*, because unlike *ibi1* mutants, *oki1* mutants were not hypersensitive to BABA (Fig. S6). Another hypothesis is that disruption in mitochondrial translation could create a redox unbalance, common in mutations that affect mitochondrial function (Mignolet-Spruyt et al. 2016). Recently, roles for redox signaling in shoot and root meristem size control have been discovered. For example, histological staining found different types of reactive oxygen species (ROS) enriched in different shoot meristem domains; superoxide is enriched in the stem cells and promotes WUS expression, and differentiation is promoted in the peripheral zone by hydrogen peroxide. The function of these ROS species is illustrated by different mutants affecting ROS status, which have shoot meristem size defects (Zeng et al. 2017). Similar findings have been reported in rice, where a glutamyl-tRNA synthetase expressed in meristematic cell layers during anther development maintains cellular organization and regulates the population of male germ cells through the control of protein synthesis, metabolic homeostasis and redox status (Yang et al.

2018). The size of root meristems is also controlled by a redox mechanism, for example the UPBEAT1 transcription factor controls the balance between cell proliferation and differentiation, by controlling expression of peroxidase gene targets (Tsukagoshi et al. 2010). Redox control of meristem size in maize is also evident, as the glutaredoxin enzyme MALE STERILE CONVERTED ANTHER1 (MSCA1) controls activity of the FASCIATED EAR4 (FEA4) transcription factor (Yang et al. 2015). The *Aberrant phyllotaxy2* (*Abph2*) mutant has bigger meristems and is caused by dominant mutations in *MSCA1*, and *msca1* loss of function mutants have smaller shoot meristems (Yang et al. 2015). Redox signaling can also control shoot meristem size by modulation of plasmodesmata, for example severe changes in redox state in the *Arabidopsis gfp aberrant trafficking1* (*gat1*) mutant of *Arabidopsis* lead to a reduction in root meristem size and premature shoot meristem termination, presumably because of excessive callose deposition, potentially impacting the flow of nutrients and developmental signals (Benitez-Alfonso et al. 2009). As described above, *oki1* has a mutation in a domain of AspRS that recognizes the anti-codon in the mRNA by charged tRNA (Mirande 2017). Therefore mitochondrial translation may be affected by the *oki1* mutation, leading to dysfunction of mitochondria (Robles and Quesada 2017; Sissler et al. 2017; Vargas-Rodriguez et al. 2018). As one of their functions, mitochondria produce ROS through oxidative phosphorylation, and in turn, those ROS signals affect transcription factors that affect meristem size and the cell cycle (Schippers et al. 2016). Thus, OKI1 may be required for the normal mitochondrial translation and functions, which allows the proper ROS metabolism in the meristem, resulting in its normal development. We note, however, that the causal relationship between ROS overaccumulation and the enlarged SAM phenotype in *oki1* is still unclear. Since we observed accumulation of ROS in *oki1* mutants that already established an enlarged SAM (Fig. 5), it is possible that the

disturbed SAM organization in *oki1* causes ROS overaccumulation indirectly. A time-course study of ROS levels in the *oki1* SAM may help better understand any causal relationship. Additionally, as an alternative possibility of OKI1 mechanism, OKI1 may interact with other proteins to function in regulating SAM size. As described above, aaRSs are involved in various essential cellular processes, and are thought to act as hub proteins that have a wide impact on cellular mechanisms beyond translation (Guo et al. 2010). In many cases, these non-canonical functions derive from the interactions of aaRSs with partner proteins (Hausmann and Ibba 2008; Havrylenko and Mirande 2015; Kekez et al. 2019; Kim et al. 2014; Laporte et al. 2014). For example, recent work indicated that *Arabidopsis* cytoplasmic seryl-tRNA synthetase (SerRS) interacts with BRI 1-5 ENHANCED 1 (BEN1) that is involved in metabolism of brassinosteroid hormones (Kekez et al. 2019). Thus, OKI1 may also interact with proteins that catalyze the metabolism of hormones to control SAM size. Further study should elucidate the precise mechanism of OKI1 in redox imbalance or interaction with meristem regulators and their roles in meristem size control.

Materials and Methods

Plant materials and growth conditions

Mutagenesis in *Arabidopsis* Col-0 was performed as described previously (Xu et al. 2011). The M1 progeny were allowed to self-fertilize, and mutants screened in the M2 population. The following lines were obtained from the Arabidopsis Biological Resource Center: *clv3-2* (Ler ecotype) (Fletcher et al. 1999), SAIL_358_B08 and the double transgenic line expressing *CLV3*::*mGFP5-ER* and *WUS*::*dsRED-N7* (Ler ecotype) (Gordon et al. 2007). *wus* mutant line (Ler ecotype) was kindly provided from Dr. Yuval Eshed (Weizmann Institute of Science, Israel). This allele in which a T-DNA is inserted into *wus* was found as part of an enhancer trap population screen (Eshed et al. 1999). *ibi1-1* mutant line (Col-0 ecotype) was kindly provided from Dr. Jurriaan Ton (The University of Sheffield, UK). *WUS::GUS* line was kindly provided by Dr. Damianos Skopelitis (Cold Spring Harbor Laboratory, USA) (Skopelitis et al. 2018).

For all experiments except Fig. 4A-H, Col-0 ecotype was used as a control line or WT. All plants were grown on soil or Murashige and Skoog (MS) agar plates (Weigel and Glazebrook 2002) at 23°C under long-day (LD, 16 h light/8 h dark) conditions. *Arabidopsis* seeds were stratified on soil or MS plates in the dark at 4°C for 48-72 h before transferring them to growth conditions. Transgenic *Arabidopsis* was obtained by *Agrobacterium*-mediated floral dip (Alonso and Stepanova 2014; Weigel and Glazebrook 2002). *wus; oki1* and *clv3-2; oki1* double mutants, and *CLV3*::*mGFP5-ER; WUS*::*dsRED-N7* in *oki1* lines were generated through genetic crosses, and identified in the F2 segregating populations. *oki1/SAIL_358_B08* mutants were generated through genetic crosses and identified in the F1. SAIL_358_B08 is listed as having T-DNA insertions in two gene loci, AT4G33760 and AT4G22860 (https://arabidopsis.org). We selected

plants that had T-DNA insertion only within AT4G33760 by PCR genotyping, and used them for the genetic crosses. *oki1* and *clv3-2* were validated based on PCR genotyping. *wus* was identified by Basta screening and PCR genotyping, and *CLV3*::*mGFP5-ER WUS*::*dsRED-N7* were validated by GFP or dsRED detection by fluorescence microscopy. Primers used for genotyping are listed in Table S1. *wus*, *clv3-2* and *CLV3*::*mGFP5-ER WUS*::*dsRED-N7* lines were from the Ler background, and *oki1* from Col-0, and double mutants were analyzed in the F3 generation. We analyzed a large number to double mutants to avoid the possibility that modifiers segregating in the mixed genetic background would affect the results.

Gene mapping

The *oki1* mutant (Col-0 ecotype) was crossed to the Ler ecotype. The F1 progeny were allowed to self-fertilize, and in the F2 population *oki1* phenotype (Fig. 1B) segregated 3:1. DNA was collected from pooled *oki1*- and WT-like plants. Library preparation was carried out according to manufacturers instructions (NEB Next Ultra DNA Library Prep Kit for Illumina, New England BioLabs Inc) and paired end sequencing was performed on the Illumina platform at the Cold Spring Harbor laboratory (New York, USA). Sequencing data was analyzed with the short read analysis pipeline SHOREmap (Schneeberger et al. 2009). Reads were aligned to the *Arabidopsis* Col-0 reference genome (TAIR 10). SNPs detected by sequencing were converted to CAPS or dCAPS markers, and a final mapping interval supported by several recombinants on each side was defined by markers at 15.65 Mb and 16.34 Mb in the Col-0 reference genome.

Molecular biology

Recombineering lines containing OKI1 fused to three copies of YPet (a YFP variant) (Nguyen and Daugherty 2005) at the C terminus (OKI1-3xYPet) or mutated OKI1 were generated using bacterial homologous recombination as described (Alonso and Stepanova 2014; Zhou et al. 2011). TAC clone JAtY59F05 and the plasmids containing recombineering cassettes with 3xYPet (3xAraYPet-FRT-Amp^R-FRT) or mCherry (mCherry-FRT-Amp^R-FRT) were kindly provided by Dr. Jose Alonso (North Carolina State University, USA). The *Escherichia coli* (*E. coli*) recombineering strain SW105 was from the National Cancer Institute (Maryland, USA). For generating 3xYPet fused OKI1, 3xAraYPet-FRT-Amp^R-FRT cassette was PCR amplified using primers 1 and 2 (Table S1) and inserted in front of stop codon in *OKI1* gene in the TAC. *E.coli* cells harboring the recombinant TAC clone was then cultured on medium containing L-arabinose, which induces FRT recombinase thus deleting the *Amp^R* gene leaving *OKI1-3xYPet* in the recombinant TAC. For generating mutated *OKI1* gene, mCherry-FRT-Amp^R-FRT cassette was PCR amplified using primers 3 and 4 (Table S1) and was inserted in a short region (26-bp; AATGTGGTGAAGCTGATTAGGAGATA) in the fourth exon of the *OKI1* gene. These clones were confirmed by sequencing using primers 5 and 6 (OKI-3xYPet) and 7 and 8 (mutated OKI1) and in turn were transformed into *Agrobacterium tumefaciens* (GV3101). Transgenic plants were screened by Basta selection.

Shoot apical meristem (SAM) measurement

SAM measurement was performed as described previously (Balkunde et al. 2017). Briefly, *Arabidopsis* seedlings were harvested at 8 or 12 DAP under LD conditions and then fixed

overnight in ice-cold FAA (10% formalin, 45% ethanol and 5% acetic acid) followed by dehydration through an ethanol series, and cleared with methyl salicylate (Sigma-Aldrich). Meristems were observed using Nomarski optics. The width and height of the meristems were measured and quantified using ImageJ-Fiji (Schindelin et al. 2012).

Chemical staining

For Eosin Y staining of cells in the SAM, 10 DAP seedlings of WT and *oki1* were fixed in FAA (5% formalin, 5% glacial acetic acid, 45% ethanol) overnight at 4°C followed by dehydration through a 50-100% ethanol series. During the dehydration step, tissues were stained with 0.1% Eosin Y (Sigma-Aldrich) in 100% ethanol, and embedded into paraffin (PARAPLAST X-TRA; McCormick SCIENTIFIC). Sections (10 μm) were prepared using a microtome. For propidium iodide (PI) staining of cell wall in the root, the roots of WT and *oki1* were stained in 10 μg/ml PI for 5 minutes, rinsed and mounted in water.

For mitochondrial staining, protoplasts were isolated from rosette leaves of 2-week old transformants that expressed OKI1::3xYPet driven under *OKI1* native promoter in *oki1* background using an enzyme solution (400 mM mannitol, 20 mM MES, 20 mM KCl, 10 mM $CaCl_2$, 10 μg/ml BSA, 15 mg/ml cellulase [PhytoTechnology Laboratories], 3 mg/ml pectolyase [Sigma-Aldrich]). Isolated protoplasts were suspended in buffer (400 mM mannitol, 20 mM MES, 20 mM KCl, 10 mM $CaCl_2$, 10 μg/ml BSA) containing 100 nM MitoTracker Red CMXRos (Molecular Probes) for mitochondrial staining. For staining in the SAM, shoot apices were embedded in 6% agar blocks, and sections were obtained with a vibratome and stained with MitoTracker Red CMXRos in PBS for 30 min.

For staining of ROS, superoxide anions and hydrogen peroxide, nitroblue tetrazolium (NBT) (Sigma-Aldrich) and 3,3'-diaminobenzidine (DAB) (Sigma-Aldrich) were used as described previously (Zeng et al. 2017). Briefly, 12 DAP seedlings were infiltrated with 1/2 liquid MS and either 1 mg/ml NBT and 50 mM potassium dihydrogen phosphate (pH 7.6) (for superoxide anion detection) or 1 mg/ml DAB and 10 mM disodium hydrogen phosphate (pH 6.5) (for hydrogen peroxide detection), and incubated in the dark for 10-20 h at room temperature. Stained plants were transferred into boiling ethanol/glycerin/glacial acetic acid solution (3:1:1) to terminate the staining, then fixed with paraformaldehyde (PFA) solution (2% paraformaldehyde, 0.1% DMSO in PBS) and embedded into 6% agar blocks for sectioning with a vibratome.

Microscopy

Seedling images were taken with Nikon SMZ1500 (Nikon Instrument Inc) microscope to manually capture Z series, which were then merged using NIS elements to create focused images. Confocal images were obtained on a ZEISS LSM710 or LSM 780. For Eosin Y, 514 nm laser excitation and 538–680 nm emission spectra, for PI, 514 nm excitation and 566-718 nm emission spectra, for MitoTracker Red, 561 nm excitation and 572-621 nm emission spectra, for YPet, 514 nm excitation and 519-588 nm emission spectra, for GFP, 488 nm excitation and 493-541 nm emission spectra, for dsRED, 594 nm excitation and 599-641 nm emission spectra, for chloroplast autofluorescence, 633 nm excitation and 647-721 nm emission spectra were used. LSM files from the confocal were processed using ImageJ-Fiji (Schindelin et al. 2012).

Multiple sequence alignment and construction of phylogenetic tree

For multiple alignment of amino acid sequences of AspRSs from eukaryotes (Fig. 2C), amino acid sequences that possess high similarity with OKI1 were obtained from National Center for Biotechnology Information (NCBI) database (https://www.ncbi.nlm.nih.gov) by BLAST search. AspRS amino acid sequences from *Arabidopsis thaliana* (OKI1, TAIR ID: AT4G33760), *Medicago truncatula* (NCBI accession number: XP_003609716), *Populus trichocarpa* (NCBI accession number: XP_024463857), *Oryza sativa* (NCBI accession number: XP_015622473), *Brachypodium distachyon* (NCBI accession number: XP_003568687), *Physcomitrella patens* (NCBI accession number: XP_02435843), *Homo sapiens* (NCBI accession number: 4AH6_A), *Drosophila melanogaster* (NCBI accession number: NP_724018), *Saccharomyces cerevisiae* (NCBI accession number: PTN17328), *Chlamydomonas reinhardtii* (NCBI accession number: XP_001694949) were used. Multiple sequence alignment was performed by CLUSTAL OMEGA (https://www.ebi.ac.uk/Tools/msa/clustalo/) (Sievers et al. 2011). For constructing a phylogenetic tree for *Arabidopsis* aaRSs (Fig. 2E), seven complete amino acid sequences that possess high similarity with OKI1 (AT5g56680, AT1G70980, AT4G17300, AT4G26870, AT4G31180, AT3G13490 and AT3G11710) were obtained from Phytozome v12.1 database (https://phytozome.jgi.doe.gov/pz/portal.html) by BLAST search. Multiple sequence alignment was performed by CLUSTALW (https://www.genome.jp/tools-bin/clustalw) (Larkin et al. 2007). Neighbor-joining (NJ) tree was constructed by MEGA 7 (Kumar et al. 2016) with 1000 bootstrap.

GUS staining

Seedlings were transferred to tissue culture plates containing GUS staining solution (50 mM Na-phosphate at pH 7.0, 10 mM EDTA, 0.1% triton X-100, 1 mg/ml of X-Gluc [5-bromo-4-chloro-

3-indolyl-beta-D-glucuronic acid, BIOSYNTH], 5mM potassium ferricyanide and 5mM potassium ferrocyanide), placed under vacuum for 5 min, and then incubated in the dark at 37 °C overnight. Staining solution was removed, and tissues were cleared in 70% ethanol.

Chemical treatment

Control line, *ibi1-1* and *oki1* seedlings were grown on MS medium plates for four days, and then transferred onto MS medium plates containing 0, 150, 500 or 1500 μM S/R-β-aminobutyric acid (Sigma-Aldrich). After ten days, the fresh weight of seedlings in each condition was measured.

Statistical analysis

Data for multiple groups were analyzed by one-way analysis of variance with a post hoc multiple comparison test (Turkey's HSD procedure) using R software (https://www.r-project.org).

Funding

This work was supported by National Science Foundation grant number [IOS-1457187] and "Next-Generation BioGreen 21 Program (System & Synthetic Agro-biotech Center, Project No. [PJ01184302])" Rural Development Administration, Republic of Korea.

Disclosures

Conflicts of interest: No conflicts of interest declared.

Acknowledgements

The authors thank Dr. Jose Alonso (North Carolina State University, USA), Dr. Yuval Eshed (Weizmann Institute of Science, Israel), Dr. Jurriaan Ton (The University of Sheffield, UK) and Dr. Damianos Skopelitis (Cold Spring Harbor Laboratory, USA) for kindly providing reagents, and Dr. Molly Hammell (Cold Spring Harbor Laboratory, USA) for assistance with sequence data analysis. The authors are also grateful to Ms. Irene Liao for assistance with genomic DNA library preparation for whole genome sequencing.

References

Alonso, J.M. and Stepanova, A.N. (2014) Arabidopsis transformation with large bacterial artificial chromosomes. In *Arabidopsis Protocols*. Edited by Sanchez-Serrano, J.J. and Salinas, J. pp. 271-283. Springer, New York.

573 Balkunde, R., Kitagawa, M., Xu, X.M., Wang, J. and Jackson, D. (2017) SHOOT
574 MERISTEMLESS trafficking controls axillary meristem formation, meristem size and organ
575 boundaries in *Arabidopsis*. *Plant J.* 90: 435-446.
576
577 Bellaoui, M. and Gruissem, W. (2004) Altered expression of the *Arabidopsis* ortholog of *DCL*
578 affects normal plant development. *Planta* 219: 819-826.
579
580 Bellaoui, M., Keddie, J.S. and Gruissem, W. (2003) DCL is a plant-specific protein required for
581 plastid ribosomal RNA processing and embryo development. *Plant Mol. Biol.* 53: 531-543.
582
583 Benitez-Alfonso, Y., Cilia, M., San Roman, A., Thomas, C., Maule, A., Hearn, S., et al. (2009)
584 Control of *Arabidopsis* meristem development by thioredoxin-dependent regulation of
585 intercellular transport. *Proc. Natl. Acad. Sci. USA* 106: 3615-3620.
586
587 Berg, M., Rogers, R., Muralla, R. and Meinke, D. (2005) Requirement of aminoacyl-tRNA
588 synthetases for gametogenesis and embryo development in *Arabidopsis*. *Plant J.* 44: 866-878.
589
590 Brand, U., Fletcher, J.C., Hobe, M., Meyerowitz, E.M. and Simon, R. (2000) Dependence of
591 stem cell fate in *Arabidopsis* on a feedback loop regulated by CLV3 activity. *Science* 289: 617-
592 619.
593
594 Byrne, M.E. (2009) A role for the ribosome in development. *Trends Plant Sci.* 14: 512-519.
595

596 Chickarmane, V.S., Gordon, S.P., Tarr, P.T., Heisler, M.G. and Meyerowitz, E.M. (2012)
597 Cytokinin signaling as a positional cue for patterning the apical–basal axis of the growing
598 *Arabidopsis* shoot meristem. *Proc. Natl. Acad. Sci. USA* 109: 4002-4007.
599
600 Chuck, G.S., Brown, P.J., Meeley, R. and Hake, S. (2014) Maize *SBP-box* transcription factors
601 *unbranched2* and *unbranched3* affect yield traits by regulating the rate of lateral primordia
602 initiation. *Proc. Natl. Acad. Sci. USA* 111: 18775-18780.
603
604 Clark, S.E., Williams, R.W. and Meyerowitz, E.M. (1997) The *CLAVATA1*gene encodes a
605 putative receptor kinase that controls shoot and floral meristem size in *Arabidopsis*. *Cell* 89: 575-
606 585.
607
608 Daum, G., Medzihradszky, A., Suzaki, T. and Lohmann, J.U. (2014) A mechanistic framework
609 for noncell autonomous stem cell induction in *Arabidopsis*. *Proc. Natl. Acad. Sci. USA* 111:
610 14619-14624.
611
612 DeYoung, B.J., Bickle, K.L., Schrage, K.J., Muskett, P., Patel, K. and Clark, S.E. (2006) The
613 CLAVATA1-related BAM1, BAM2 and BAM3 receptor kinase-like proteins are required for
614 meristem function in *Arabidopsis*. *Plant J.* 45: 1-16.
615
616 DeYoung, B.J. and Clark, S.E. (2008) BAM Receptors Regulate Stem Cell Specification and
617 Organ Development Through Complex Interactions With CLAVATA Signaling. *Genetics* 180:
618 895-904.

Dolzblasz, A., Smakowska, E., Gola, E.M., Sokolowska, K., Kicia, M. and Janska, H. (2016) The mitochondrial protease AtFTSH4 safeguards *Arabidopsis* shoot apical meristem function. *Sci. Rep.* 6: 28315.

Duchêne, A.-M., Giritch, A., Hoffmann, B., Cognat, V., Lancelin, D., Peeters, N.M., et al. (2005) Dual targeting is the rule for organellar aminoacyl-tRNA synthetases in *Arabidopsis thaliana*. *Proc. Natl. Acad. Sci. USA* 102: 16484-16489.

Eshed, Y., Baum, S.F. and Bowman, J.L. (1999) Distinct mechanisms promote polarity establishment in carpels of *Arabidopsis*. *Cell* 99: 199-209.

Fletcher, J.C., Brand, U., Running, M.P., Simon, R. and Meyerowitz, E.M. (1999) Signaling of cell fate decisions by *CLAVATA3* in *Arabidopsis* shoot meristems. *Science* 283: 1911-1914.

Gordon, S.P., Chickarmane, V.S., Ohno, C. and Meyerowitz, E.M. (2009) Multiple feedback loops through cytokinin signaling control stem cell number within the *Arabidopsis* shoot meristem. *Proc. Natl. Acad. Sci. USA* 106: 16529-16534.

Gordon, S.P., Heisler, M.G., Reddy, G.V., Ohno, C., Das, P. and Meyerowitz, E.M. (2007) Pattern formation during de novo assembly of the *Arabidopsis* shoot meristem. *Development* 134: 3539-3548.

642 Graf, P., Dolzblasz, A., Würschum, T., Lenhard, M., Pfreundt, U. and Laux, T. (2010) *MGOUN1*
643 encodes an *Arabidopsis* type IB DNA topoisomerase required in stem cell regulation and to
644 maintain developmentally regulated gene silencing. *Plant Cell* 22: 716-728.
645
646 Gruel, J., Landrein, B., Tarr, P., Schuster, C., Refahi, Y., Sampathkumar, A., et al. (2016) An
647 epidermis-driven mechanism positions and scales stem cell niches in plants. *Sci. Adv.* 2:
648 e1500989.
649
650 Guo, M., Yang, X.L. and Schimmel, P. (2010) New functions of aminoacyl-tRNA synthetases
651 beyond translation. *Nat. Rev. Mol. Cell Biol.* 11: 668-674.
652
653 Hausmann, C.D. and Ibba, M. (2008) Aminoacyl-tRNA synthetase complexes: molecular
654 multitasking revealed. *Fems Microbiol. Rev.* 32: 705-721.
655
656 Havrylenko, S. and Mirande, M. (2015) Aminoacyl-tRNA synthetase complexes in evolution. *Int.*
657 *J. Mol. Sci.* 16: 6571-6594.
658
659 Hu, C., Zhu, Y., Cui, Y., Cheng, K., Liang, W., Wei, Z., et al. (2018) A group of receptor kinases
660 are essential for CLAVATA signalling to maintain stem cell homeostasis. *Nat. Plants* 4: 205.
661
662 Huang, S.B., Van Aken, O., Schwarzlander, M., Belt, K. and Millar, A.H. (2016) The roles of
663 mitochondrial reactive oxygen species in cellular signaling and stress response in plants. *Plant*
664 *Physiol.* 171: 1551-1559.

Jiang, K., Meng, Y.L. and Feldman, L.J. (2003) Quiescent center formation in maize roots is associated with an auxin-regulated oxidizing environment. *Development* 130: 1429-1438.

Kaya, H., Shibahara, K.-i., Taoka, K.-i., Iwabuchi, M., Stillman, B. and Araki, T. (2001) *FASCIATA* genes for chromatin assembly factor-1 in *Arabidopsis* maintain the cellular organization of apical meristems. *Cell* 104: 131-142.

Kayes, J.M. and Clark, S.E. (1998) *CLAVATA2*, a regulator of meristem and organ development in *Arabidopsis*. *Development* 125: 3843-3851.

Kekez, M., Zanki, V., Kekez, I., Baranasic, J., Hodnik, V., Duchene, A.M., et al. (2019) *Arabidopsis* seryl-tRNA synthetase: the first crystal structure and novel protein interactor of plant aminoacyl-tRNA synthetase. *Febs J.* 286: 536-554.

Kim, J.H., Han, J.M. and Kim, S. (2014) Protein-protein interactions and multi-component complexes of aminoacyl-tRNA synthetases. In *Aminoacyl-Trna Synthetases in Biology and Medicine*. Edited by Kim, S. pp. 119-144. Springer-Verlag Berlin, Berlin.

Kong, X.P., Tian, H.Y., Yu, Q.Q., Zhang, F., Wang, R., Gao, S., et al. (2018) PHB3 maintains root stem cell niche identity through ROS-responsive AP2/ERF transcription factors in *Arabidopsis*. *Cell Rep.* 22: 1350-1363.

688 Kumar, S., Stecher, G. and Tamura, K. (2016) MEGA7: Molecular evolutionary genetics
689 analysis version 7.0 for bigger datasets. *Mol. Biol. Evol.* 33: 1870-1874.
690
691 Landrein, B., Formosa-Jordan, P., Malivert, A., Schuster, C., Melnyk, C.W., Yang, W., et al.
692 (2018) Nitrate modulates stem cell dynamics in *Arabidopsis* shoot meristems through cytokinins.
693 *Proc. Natl. Acad. Sci. USA* 115: 1382-1387.
694
695 Landrein, B., Refahi, Y., Besnard, F., Hervieux, N., Mirabet, V., Boudaoud, A., et al. (2014)
696 Meristem size contributes to the robustness of phyllotaxis in *Arabidopsis*. *J. Exp. Bot.* 66: 1317-
697 1324.
698
699 Laporte, D., Huot, J.L., Bader, G., Enkler, L., Senger, B. and Becker, H.D. (2014) Exploring the
700 evolutionary diversity and assembly modes of multi-aminoacyl-tRNA synthetase complexes:
701 Lessons from unicellular organisms. *FEBS Lett.* 588: 4268-4278.
702
703 Larkin, M.A., Blackshields, G., Brown, N.P., Chenna, R., McGettigan, P.A., McWilliam, H., et
704 al. (2007) Clustal W and clustal X version 2.0. *Bioinformatics* 23: 2947-2948.
705
706 Luna, E., Van Hulten, M., Zhang, Y., Berkowitz, O., López, A., Pétriacq, P., et al. (2014) Plant
707 perception of β-aminobutyric acid is mediated by an aspartyl-tRNA synthetase. *Nat. Chem. Biol.*
708 10: 450-456.
709

710 Mayer, K.F., Schoof, H., Haecker, A., Lenhard, M., Jürgens, G. and Laux, T. (1998) Role of
711 *WUSCHEL* in regulating stem cell fate in the *Arabidopsis* shoot meristem. *Cell* 95: 805-815.
712
713 Mignolet-Spruyt, L., Xu, E.J., Idanheimo, N., Hoeberichts, F.A., Muhlenbock, P., Brosche, M.,
714 et al. (2016) Spreading the news: subcellular and organellar reactive oxygen species production
715 and signalling. *J. Exp. Bot.* 67: 3831-3844.
716
717 Mirande, M. (2017) The aminoacyl-tRNA synthetase complex. In *Macromolecular Protein*
718 *Complexes*. Edited by Harris, J.R. and Marles-Wright, J. pp. 505-522. Springer, New York.
719
720 Miwa, H., Betsuyaku, S., Iwamoto, K., Kinoshita, A., Fukuda, H. and Sawa, S. (2008) The
721 Receptor-Like Kinase SOL2 Mediates CLE Signaling in *Arabidopsis*. *Plant Cell Physiol.* 49:
722 1752-1757.
723
724 Moschopoulos, A., Derbyshire, P. and Byrne, M.E. (2012) The *Arabidopsis* organelle-localized
725 glycyl-tRNA synthetase encoded by *EMBRYO DEFECTIVE DEVELOPMENT1* is required for
726 organ patterning. *J. Exp. Bot.* 63: 5233-5243.
727
728 Muller, R., Bleckmann, A. and Simon, R. (2008) The receptor kinase CORYNE of *Arabidopsis*
729 transmits the stem cell-limiting signal CLAVATA3 independently of CLAVATA1. *Plant Cell*
730 20: 934-946.
731

Nimchuk, Z.L., Tarr, P.T. and Meyerowitz, E.M. (2011) An evolutionarily conserved pseudokinase mediates stem cell production in plants. *Plant Cell* 23: 851-854.

Nimchuk, Z.L., Zhou, Y., Tarr, P.T., Peterson, B.A. and Meyerowitz, E.M. (2015) Plant stem cell maintenance by transcriptional cross-regulation of related receptor kinases. *Development* 142: 1043-1049.

Ogawa, M., Shinohara, H., Sakagami, Y. and Matsubayashi, Y. (2008) *Arabidopsis* CLV3 peptide directly binds CLV1 ectodomain. *Science* 319: 294-294.

Pautler, M., Eveland, A.L., LaRue, T., Yang, F., Weeks, R., Je, B.I., et al. (2015) *FASCIATED EAR4* encodes a bZIP transcription factor that regulates shoot meristem size in maize. *Plant Cell* 27: 104-120.

Perales, M., Rodriguez, K., Snipes, S., Yadav, R.K., Diaz-Mendoza, M. and Reddy, G.V. (2016) Threshold-dependent transcriptional discrimination underlies stem cell homeostasis. *Proc. Natl. Acad. Sci. USA* 113: E6298-E6306.

Pinon, V., Etchells, J.P., Rossignol, P., Collier, S.A., Arroyo, J.M., Martienssen, R.A., et al. (2008) Three *PIGGYBACK* genes that specifically influence leaf patterning encode ribosomal proteins. *Development* 135: 1315-1324.

754 Robles, P. and Quesada, V. (2017) Emerging roles of mitochondrial ribosomal proteins in plant
755 Development. *Int. J. Mol. Sci.* 18: 2595.
756
757 Schimmel, P. (2018) The emerging complexity of the tRNA world: Mammalian tRNAs beyond
758 protein synthesis. *Nat. Rev. Mol. Cell Biol.* 19: 45-58.
759
760 Schindelin, J., Arganda-Carreras, I., Frise, E., Kaynig, V., Longair, M., Pietzsch, T., et al. (2012)
761 Fiji: an open-source platform for biological-image analysis. *Nat. Methods* 9: 676-682.
762
763 Schippers, J.H.M., Foyer, C.H. and van Dongen, J.T. (2016) Redox regulation in shoot growth,
764 SAM maintenance and flowering. *Curr. Opin. Plant Biol.* 29: 121-128.
765
766 Schneeberger, K., Ossowski, S., Lanz, C., Juul, T., Petersen, A.H., Nielsen, K.L., et al. (2009)
767 SHOREmap: simultaneous mapping and mutation identification by deep sequencing. *Nat.*
768 *Methods* 6: 550.
769
770 Schoof, H., Lenhard, M., Haecker, A., Mayer, K.F., Jürgens, G. and Laux, T. (2000) The stem
771 cell population of *Arabidopsis* shoot meristems is maintained by a regulatory loop between the
772 *CLAVATA* and *WUSCHEL* genes. *Cell* 100: 635-644.
773
774 Shi, B., Guo, X., Wang, Y., Xiong, Y., Wang, J., Hayashi, K.-i., et al. (2018) Feedback from
775 lateral organs controls shoot apical meristem growth by modulating auxin transport. *Dev. cell* 44:
776 204-216.

Shinohara, H. and Matsubayashi, Y. (2015) Reevaluation of the CLV3-receptor interaction in the shoot apical meristem: dissection of the CLV3 signaling pathway from a direct ligand-binding point of view. *Plant J.* 82: 328-336.

Sievers, F., Wilm, A., Dineen, D., Gibson, T.J., Karplus, K., Li, W.Z., et al. (2011) Fast, scalable generation of high-quality protein multiple sequence alignments using Clustal Omega. *Mol. Syst. Biol.* 7: 539.

Sissler, M., Gonzalez-Serrano, L.E. and Westhof, E. (2017) Recent advances in mitochondrial aminoacyl-tRNA synthetases and disease. *Trends Mol. Med* 23: 693-708.

Skopelitis, D.S., Hill, K., Klesen, S., Marcos, C.F., von Born, P., Chitwood, D.H., et al. (2018) Gating of miRNA movement at defined cell-cell interfaces governs their impact as positional signals. *Nat. Commun.* 9: 3107.

Smith, L.G., Hake, S. and Sylvester, A.W. (1996) The *tangled-1* mutation alters cell division orientations throughout maize leaf development without altering leaf shape. *Development* 122: 481-489.

Somssich, M., Je, B.I., Simon, R. and Jackson, D. (2016) CLAVATA-WUSCHEL signaling in the shoot meristem. *Development* 143: 3238-3248.

800 Tsukagoshi, H., Busch, W. and Benfey, P.N. (2010) Transcriptional regulation of ROS controls
801 transition from proliferation to differentiation in the root. *Cell* 143: 606-616.
802
803 Vargas-Rodriguez, O., Sevostyanova, A., Söll, D. and Crnković, A. (2018) Upgrading
804 aminoacyl-tRNA synthetases for genetic code expansion. *Curr. Opin. Chem. Biol.* 46: 115-122.
805
806 Weigel, D. and Glazebrook, J. (2002) *Arabidopsis*: a laboratory manual. CSHL Press.
807
808 Wilson, M.E., Mixdorf, M., Berg, R.H. and Haswell, E.S. (2016) Plastid osmotic stress
809 influences cell differentiation at the plant shoot apex. *Development* 143: 3382-3393.
810
811 Xu, X.M., Wang, J., Xuan, Z.Y., Goldshmidt, A., Borrill, P.G.M., Hariharan, N., et al. (2011)
812 Chaperonins Facilitate KNOTTED1 Cell-to-Cell Trafficking and Stem Cell Function. *Science*
813 333: 1141-1144.
814
815 Yadav, R.K., Perales, M., Gruel, J., Girke, T., Jönsson, H. and Reddy, G.V. (2011) WUSCHEL
816 protein movement mediates stem cell homeostasis in the *Arabidopsis* shoot apex. *Genes Dev.* 25:
817 2025-2030.
818
819 Yang, F., Bui, H.T., Pautler, M., Llaca, V., Johnston, R., Lee, B.-h., et al. (2015) A maize
820 glutaredoxin gene, *Abphyl2*, regulates shoot meristem size and phyllotaxy. *Plant Cell* 27: 121-
821 131.
822

823 Yang, L., Zhang, J., He, J.N., Qin, Y.Y., Hua, D.P., Duan, Y., et al. (2014) ABA-mediated ROS
824 in mitochondria regulate root meristem activity by controlling *PLETHORA* expression in
825 *Arabidopsis*. *PLoS Genet.* 10: e1004791.
826
827 Yang, X., Li, G., Tian, Y., Song, Y., Liang, W. and Zhang, D. (2018) A rice glutamyl-tRNA
828 synthetase modulates early anther cell division and patterning. *Plant Physiol.* 177: 728-744.
829
830 Yu, Q.Q., Tian, H.Y., Yue, K., Liu, J.J., Zhang, B., Li, X.G., et al. (2016) A P-Loop NTPase
831 regulates quiescent center cell division and distal stem cell identity through the regulation of
832 ROS homeostasis in *Arabidopsis* root. *PLoS Genet.* 12: e1006175.
833
834 Yu, X., Pasternak, T., Eiblmeier, M., Ditengou, F., Kochersperger, P., Sun, J.Q., et al. (2013)
835 Plastid-localized glutathione reductase2-regulated glutathione redox status is essential for
836 *Arabidopsis* root apical meristem maintenance. *Plant Cell* 25: 4451-4468.
837
838 Zeng, J., Dong, Z., Wu, H., Tian, Z. and Zhao, Z. (2017) Redox regulation of plant stem cell fate.
839 *EMBO J.* 36: 2844-2855.
840
841 Zhao, Z., Andersen, S.U., Ljung, K., Dolezal, K., Miotk, A., Schultheiss, S.J., et al. (2010)
842 Hormonal control of the shoot stem-cell niche. *Nature* 465: 1089-1092.
843

844 Zheng, M., Wang, Y., Liu, X., Sun, J., Wang, Y., Xu, Y., et al. (2016) The *RICE MINUTE-*
845 *LIKE1* (*RML1*) gene, encoding a ribosomal large subunit protein L3B, regulates leaf morphology
846 and plant architecture in rice. *J. Exp. Bot.* 67: 3457-3469.
847
848 Zhou, R.R., Benavente, L.M., Stepanova, A.N. and Alonso, J.M. (2011) A recombineering-based
849 gene tagging system for *Arabidopsis*. *Plant J.* 66: 712-723.
850
851

852 **Legends of figures**

853

854 **Figure 1. Shoot and root meristems are affected in *oki1* mutants.**

855 (A, B) *oki1* displayed narrower true leaves (B, arrowhead) in seedlings compared with control
856 line (Col-0, A). Scale bars = 5 mm. (C) *oki1* mutants have enlarged SAM (dashed circle). Scale
857 bar = 500 μm. (D-F) The inflorescence stems of control line (D) and *oki1* (E, F); *oki1* was often
858 fasciated (E and F). Scale bars = 2 cm (D) and 1 cm (E, F). (G, H) Cleared SAM from the control
859 line (G) and *oki1* (H) at 12 DAP. Solid and dashed double-headed lines display the SAM height
860 and diameter, respectively. Scale bar = 100 μm. (I, J) The SAM of *oki1* was significantly larger
861 at 12 DAP. N = 10-15. Bars topped by different letters are significantly different at $P < 0.01$
862 (Tukey HSD test). (K-R) Cell arrangements were disorganized in the *oki1* SAM and root tips.
863 Confocal images of Eosin Y-stained SAM sections of control line (K) and *oki1* (M), and PI-
864 stained root tips of control line (O) and *oki1* (Q). L, N, P, R show magnified images of the boxed
865 regions in K, M, O and Q, respectively. Scale bar = 50 μm (K, M, O, Q), 20 μm (L, N) and 10
866 μm (P, R).

867

868

869 **Figure 2. The causal gene of *oki1* encodes a mitochondrial aspartyl tRNA synthetase**
870 **(AspRS).** (A) Diagram of the intron-exon structure of *OKI1* gene (*At4g33760*). UTRs are
871 indicated by white boxes, coding regions of exons by grey boxes. Solid lines indicate the
872 intergenic regions and introns. The nucleotide substitution in *oki1* (G347A) is shown in red
873 arrowhead. T-DNA insertion site for SAIL_358_B08 is shown in black arrowhead. (B)
874 Schematic diagram of the domain structure of OKI1 protein. Predicted anti-codon binding

875 domain (91-176 aa) and the catalytic domain of AspRS (199-638 aa) are shown in yellow and
876 pink boxes, respectively. Glycine 116 within the anti-codon binding domain was changed to
877 aspartic acid in *oki1* mutants (red arrowhead). (C) Alignment of amino acid sequence of AspRS
878 from *Arabidopsis thaliana*, *Medicago truncatula*, *Populus trichocarpa*, *Oryza sativa,*
879 *Brachypodium distachyon*, *Physcomitrella patens*, *Chlamydomonas reinhardtii*, *Saccharomyces*
880 *cerevisiae, Drosophila melanogaster* and *Homo sapiens*. The Gly 116 that was replaced to
881 Aspartic acid in *oki1* mutant is fully conserved in plants and animals (arrowhead). (D) F1 plants
882 from crosses between *oki1* and *SAIL_358_B08* showed enhanced *oki1* narrow leaf phenotype
883 (also see Fig. S1A). (E) A phylogenetic tree of 8 aminoacyl-tRNA synthetases from *Arabidopsis*
884 conducted by MEGA7 software with the neighbor-joining (NJ) method for 1000 replicates
885 bootstrap. In *Arabidopsis*, there are three AspRSs, AT4G33760 (OKI1), AT4G26870 and
886 AT4G31180 (IBI1; Luna et al., 2014). AsnRS: Asparaginyl-tRNA synthtase, LysRS: Lysyl-
887 tRNA synthetase.
888
889 **Figure 3. OKI1 locates at mitochondria in the SAM.** (A, B) Bright field and fluorescence
890 images of the inflorescence SAM showing OKI1::3xYPet driven under its native promoter in
891 *oki1* background. pOKI1-OKI1::3xYPet is expressed in the meristem and shoot apex. Scale bar
892 = 50 µm. (C-E) Subcellular localization of OKI1::3xYPet (C), mitochondria stained with
893 MitoTracker Red (D), autofluorescence of plastids (blue) (E) in the cells of the SAM. Merged
894 images of C with D (F) and C with E (G) are shown. OKI1::3xYPet localized to mitochondria
895 (overlap shown by white arrows), but not plastids (blue) in the meristem. Scale bar = 10 µm.
896

Figure 4. Relationship of *OKI1* with known meristem signals. (A-H) Confocal images of pCLV3::mGFP5-ER (green) and pWUS::dsRED-N7 (red) in the SAM from 8 DAP (A-D) and 12 DAP (E-H) seedlings of control line (A, B, E, F) and *oki1* (C, D, G, H). Dashed lines display the outlines of the SAM. WUS and CLV3 promoter activities were enlarged in the SAM of *oki1* at 12 DAP. Scale bar = 100 μm. (I-P) *wus* and *clv3* are epistatic to *oki1*. Shoot apices of 35 DAP plants of control line (I), *oki1* (J), *wus* (K, L), *wus oki1* (M, N), *clv3-2* (O) and *clv3-2 oki1* (P). Scale bars = 5 mm (I, J, L, N, O, P), 1 cm (K, M).

Figure 5. *oki1* overaccumulates superoxide and hydrogen peroxide in the SAM. (A, B) Nitroblue tetrazolium (NBT) staining showed that superoxide is higher in the SAM of *oki1* (B, dark blue stained region within dashed circle) compared with control line (A, blue region shown by arrowhead). (C, D) 3,3'-diaminobenzidine (DAB) staining indicated that hydrogen peroxide levels were higher in the SAM of *oki1* (D, brown and black regions within dashed circle) compared with control line (C, brown regions indicated by arrowheads). Dashed lines in A and C show the outlines of the SAM of the control line. Scale bars = 100 μm.

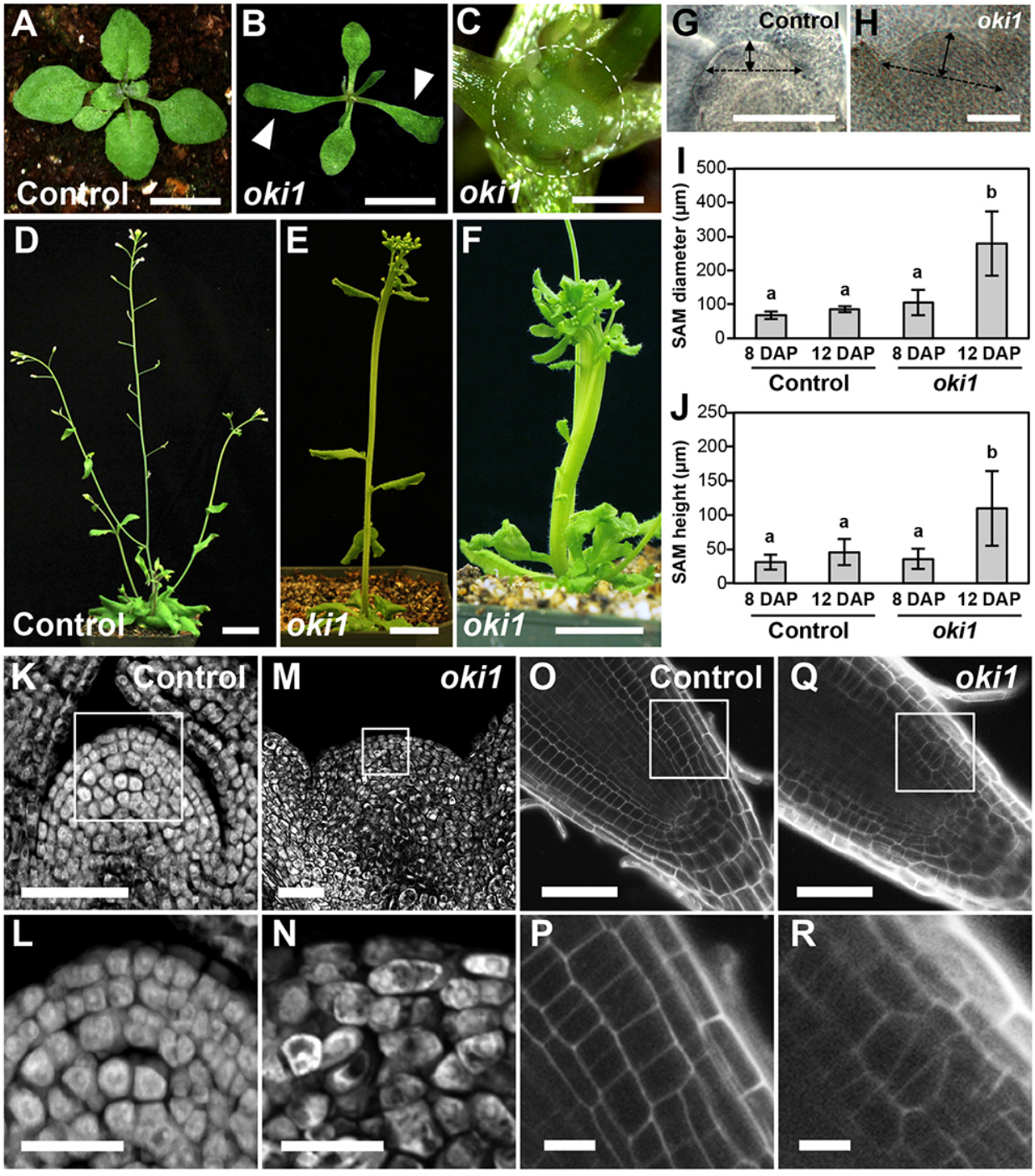
A
Control
B
oki1
C
oki1
G
Control
H
oki1
I
SAM diameter (µm)
500
400
300
200
100
0
a
a
a
b
8 DAP
12 DAP
8 DAP
12 DAP
Control
oki1
J
SAM height (µm)
250
200
150
100
50
0
a
a
a
b
8 DAP
12 DAP
8 DAP
12 DAP
Control
oki1
D
Control
E
oki1
F
oki1
K
Control
M
oki1
O
Control
Q
oki1
L
N
P
R

Figure 1

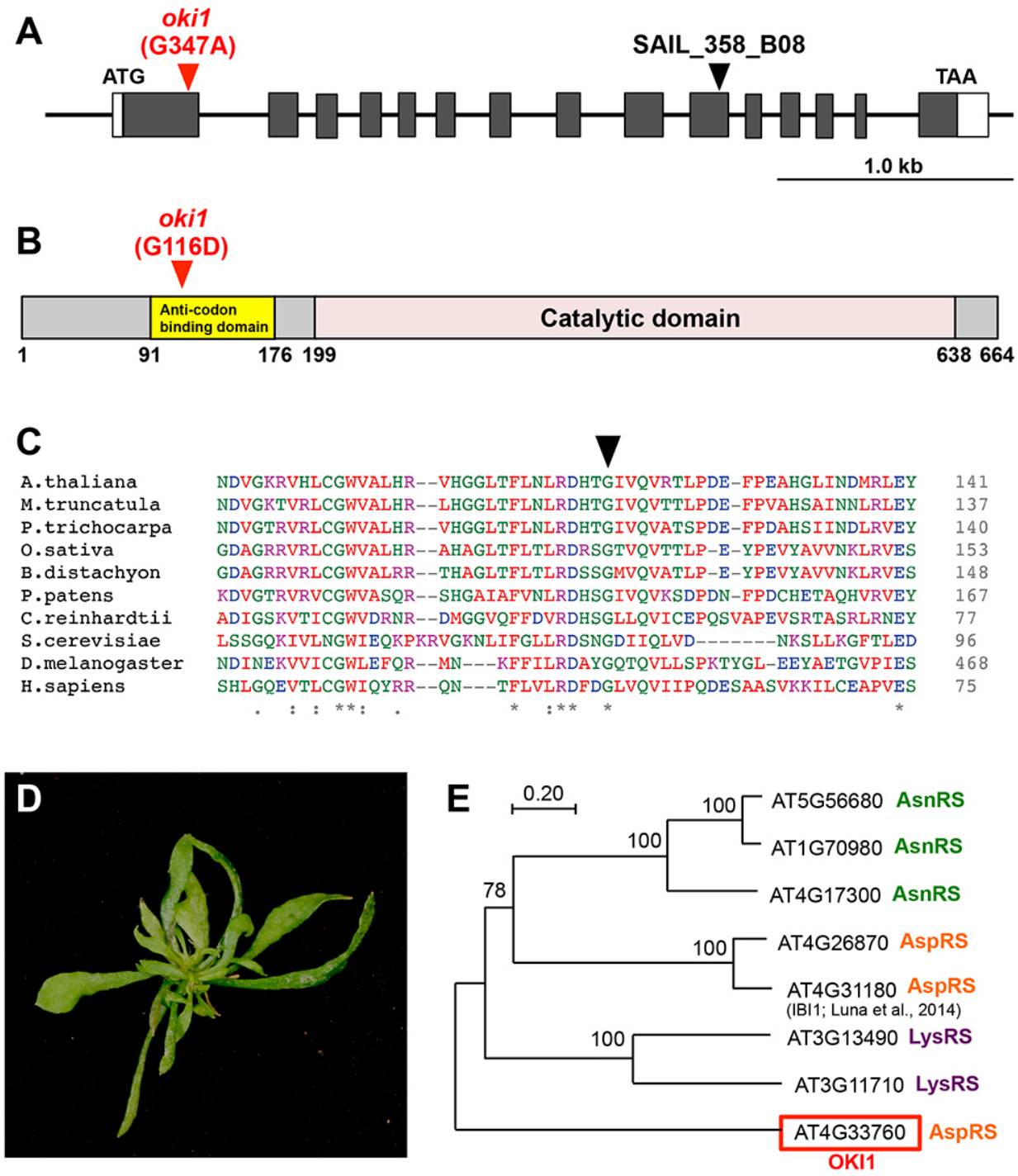
A
oki1
(G347A)
ATG
SAIL_358_B08
TAA
1.0 kb
B
oki1
(G116D)
Anti-codon
binding domain
Catalytic domain
1
91
176
199
638
664
C
A.thaliana NDVGKRVHLCGWVALHR--VHGGLTFLNLRDHTGIVQVRTLPDE-FPEAHGLINDMRLEY 141
M.truncatula NDVGKTVRLCGWVALHR--LHGGLTFLNLRDHTGIVQVTTLPDE-FPVAHSAINNLRLEY 137
P.trichocarpa NDVGTRVRLCGWVALHR--VHGGLTFLNLRDHTGIVQVATSPDE-FPDAHSIINDLRVEY 140
O.sativa GDAGRRVRLCGWVALHR--AHAGLTFLTLRDRSGTVQVTTLP-E-YPEVYAVVNKLRVES 153
B.distachyon GDAGRRVRLCGWVALRR--THAGLTFLTLRDSSGMVQVATLP-E-YPEVYAVVNKLRVES 148
P.patens KDVGTRVRVCGWVASQR--SHGAIAFVNLRDHSGIVQVKSDPDN-FPDCHETAQHVRVEY 167
C.reinhardtii ADIGSKVTICGWVDRNR--DMGGVQFFDVRDHSGLLQVICEPQSVAPEVSRTASRLRNEY 77
S.cerevisiae LSSGQKIVLNGWIEQKPKRVGKNLIFGLLRDSNGDIIQLVD--------NKSLLKGFTLED 96
D.melanogaster NDINEKVVICGWLEFQR--MN---KFFILRDAYGQTQVLLSPKTYGL-EEYAETGVPIES 468
H.sapiens SHLGQEVTLCGWIQYRR--QN---TFLVLRDFDGLVQVIIPQDESAASVKKILCEAPVES 75
D
E
0.20
100
AT5G56680 AsnRS
100
AT1G70980 AsnRS
78
AT4G17300 AsnRS
100
AT4G26870 AspRS
AT4G31180 AspRS
(IBI1; Luna et al., 2014)
100
AT3G13490 LysRS
AT3G11710 LysRS
AT4G33760 AspRS
OKI1

Figure 2

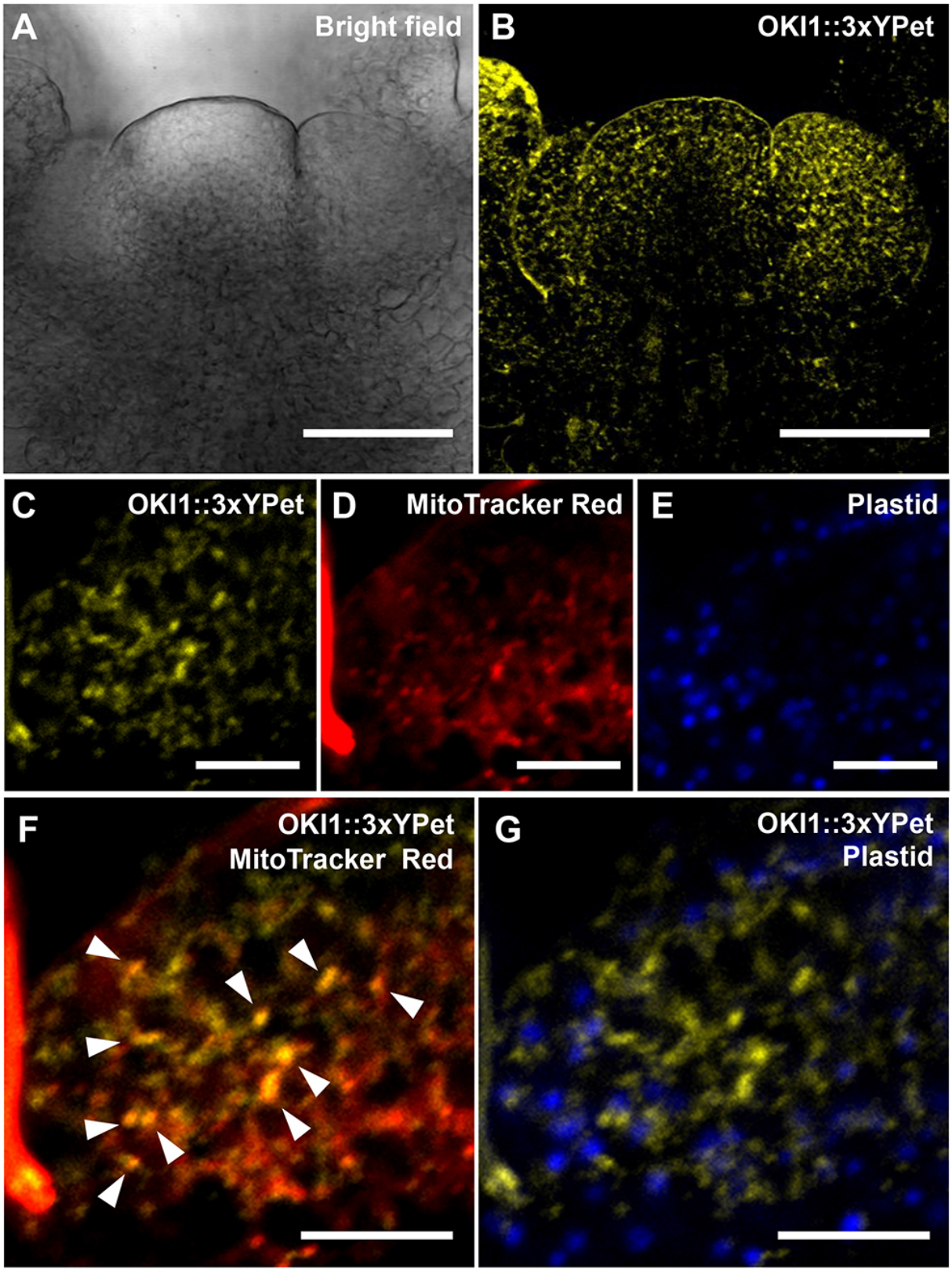

924

925 Figure 3

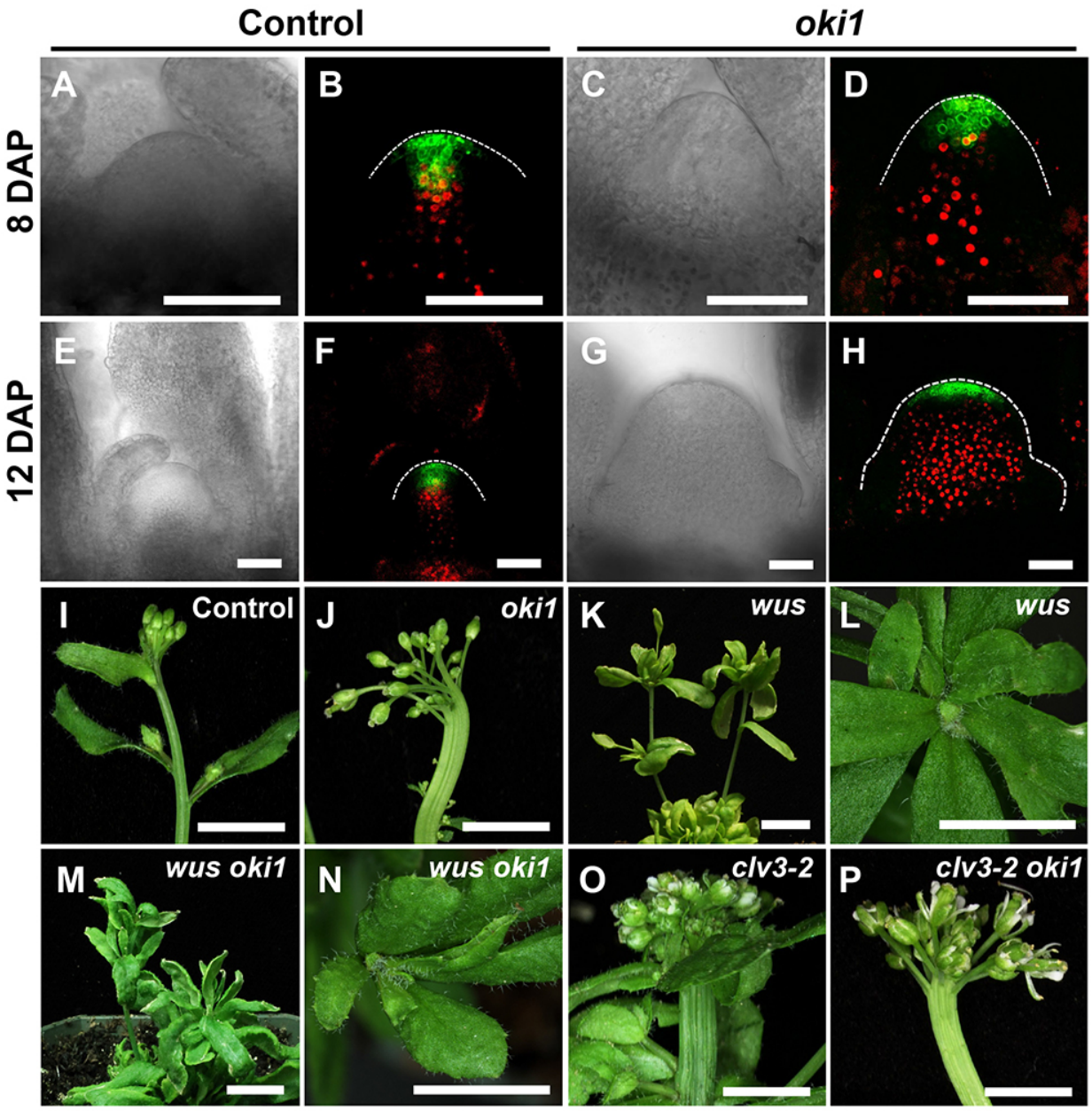
Control
oki1
8 DAP
12 DAP
A
B
C
D
E
F
G
H
I
Control
J
oki1
K
wus
L
wus
M
wus oki1
N
wus oki1
O
clv3-2
P
clv3-2 oki1

Figure 4

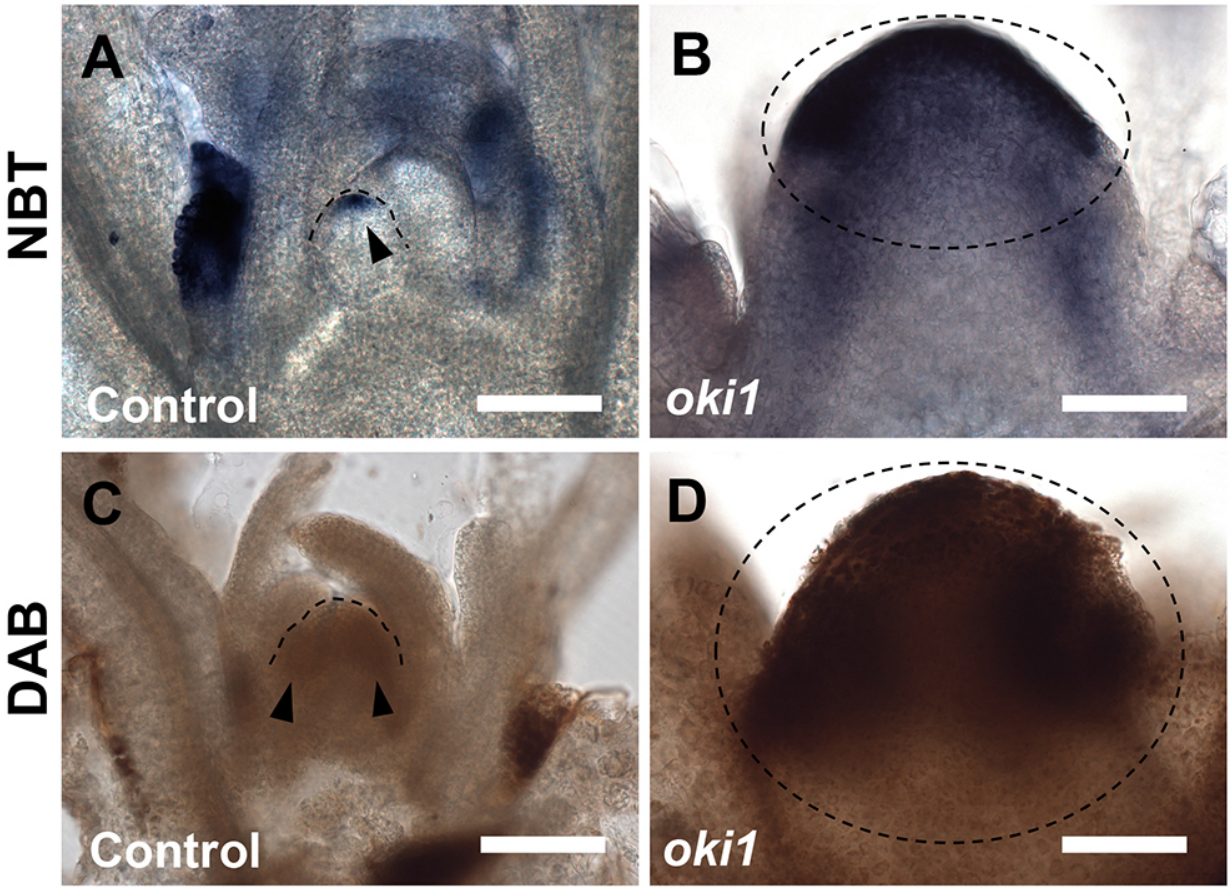

Figure 5

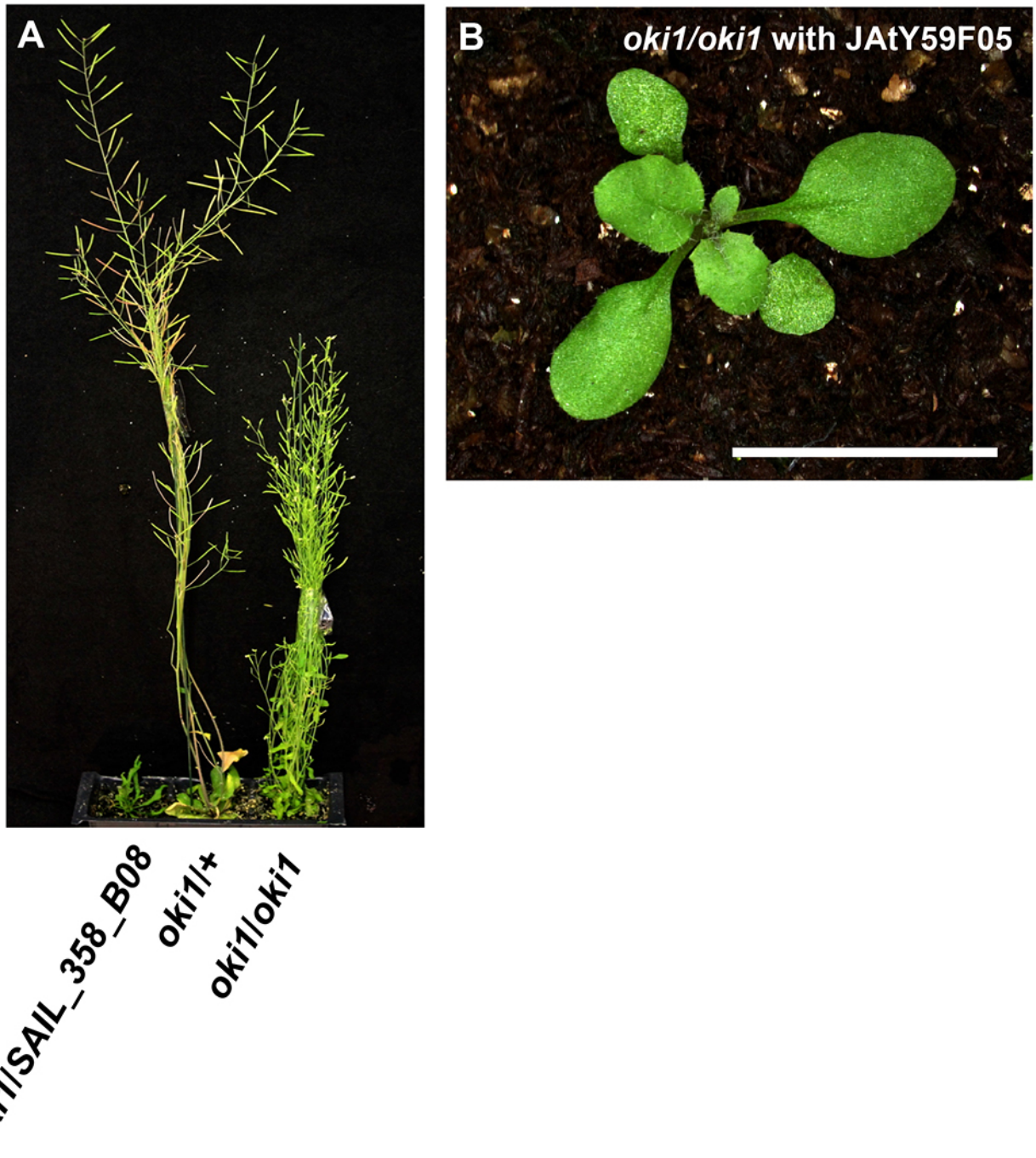

Figure S1. Genetic complementation of *oki1*. (A) *oki1*/*SAIL_358_B08* (weak allele / null) plants failed to complement *oki1*, and displayed enhanced growth defect phenotype of *oki1*. (B) Developmental phenotype of *oki1* (Fig. 1B) was complemented by introduction of TAC clone JAtY59F05 containing the *At4g33760* gene. Scale bar = 1 cm.

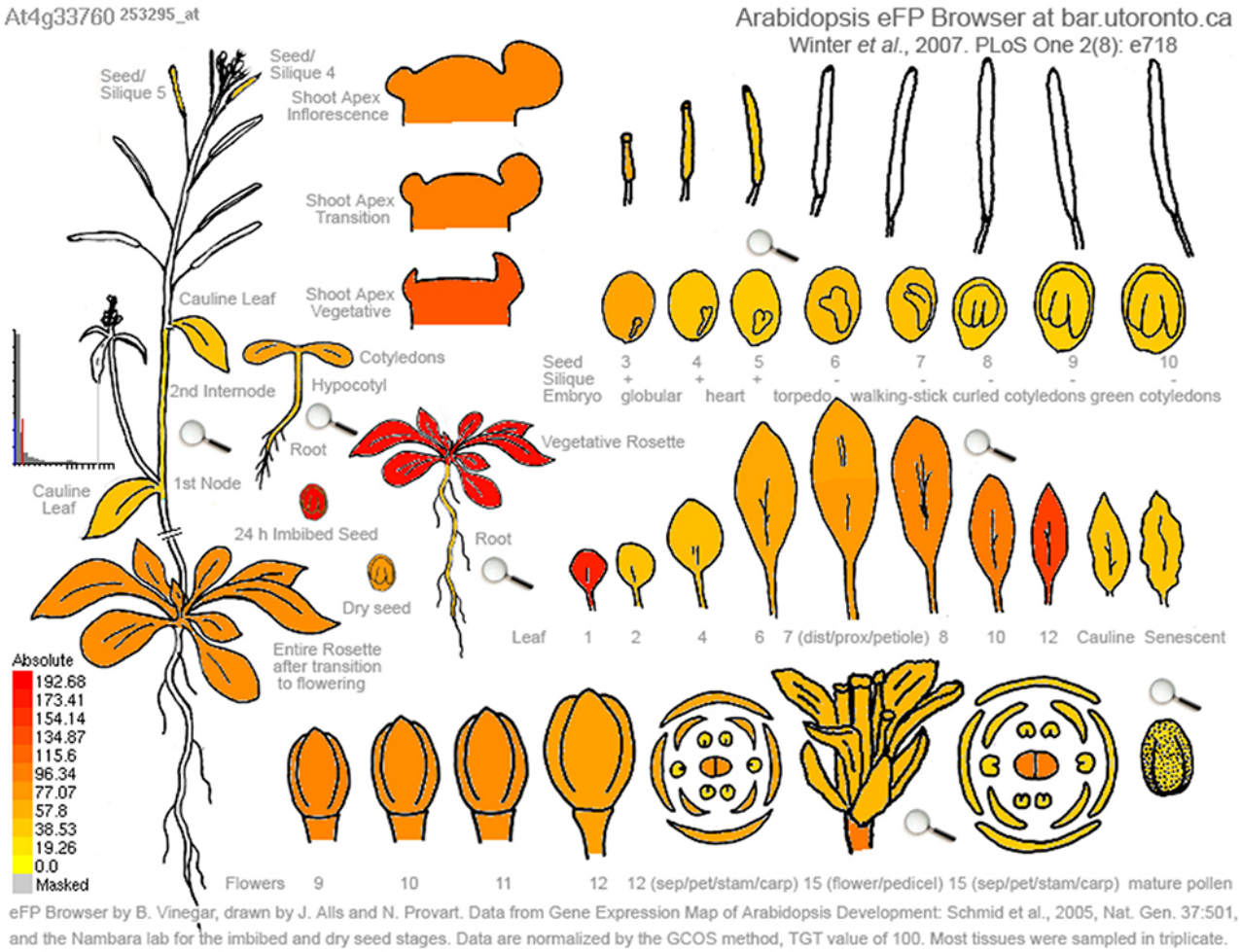

Figure S2. *OKI1* expression in *Arabidopsis* development. *OKI1* is expressed ubiquitously during *Arabidopsis* development. Figures were generated online using the eFP browser (http://bbc.botany.utoronto.ca/efp/cgi-bin/efpWeb.cgi). Relative expression levels of *OKI1* in various organs are shown via color scale, with red color indicating higher expression and yellow color indicating lower expression.

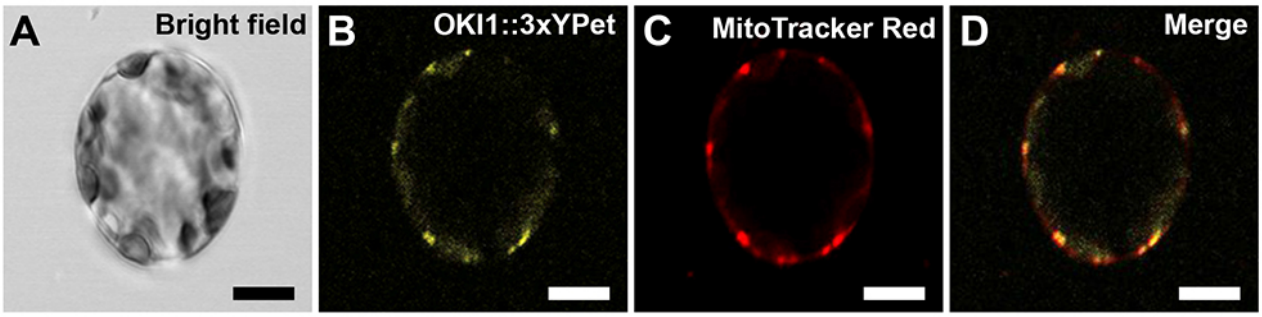

Figure S3. Mitochondrial localization of OKI1 in protoplasts derived from leaf mesophyll cells. (A) Bright field image of a protoplast derived from leaf mesophyll cells of the OKI1::3xYPet line driven by the native promoter in *oki1* background. (B) OKI1::3xYPet. (C) MitoTracker Red. (D) Merged image of B with C showed co-localization. Scale bar = 10 μm.

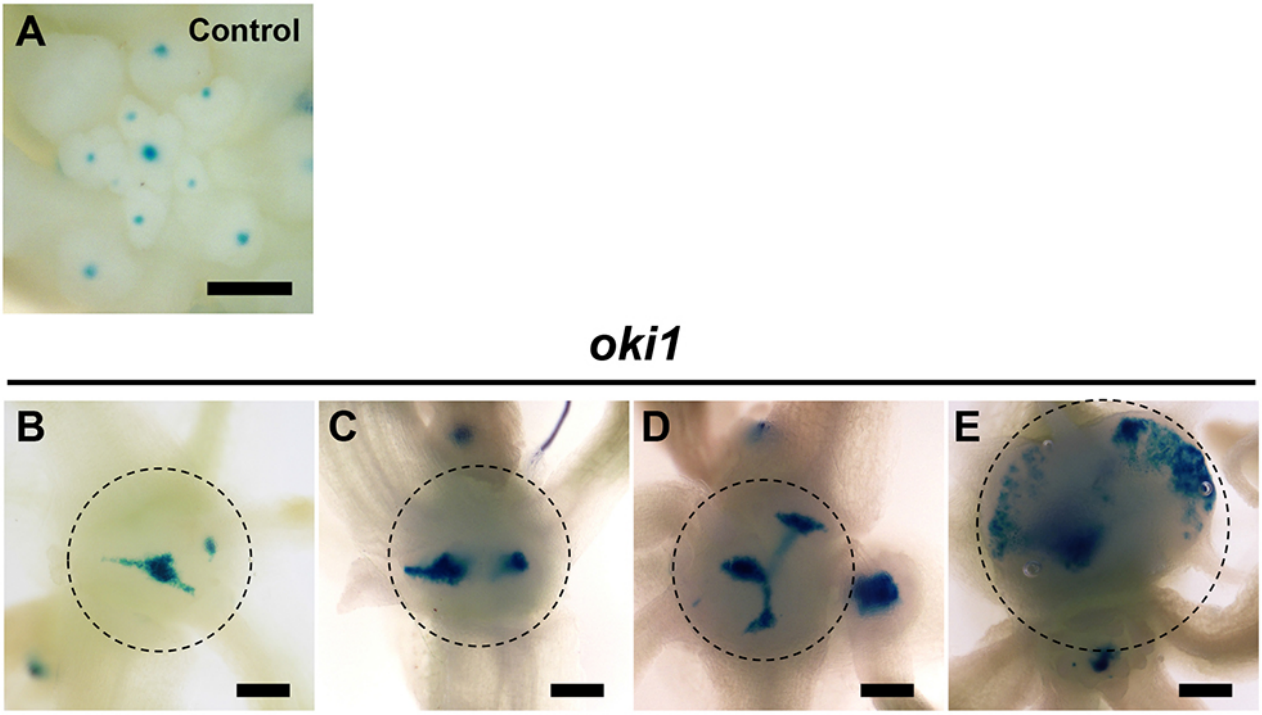

Figure S4. Abnormal WUS expression in the SAM of *oki1* mutants. (A-E) The expression patterns of promoter WUS fused GUS in control line (A) and *oki1* mutants (B-E). WUS expression site (blue region) was enlarged and/or split in the SAM of *oki1* mutants (blue regions in dashed circles). Scale bar = 200 μm.

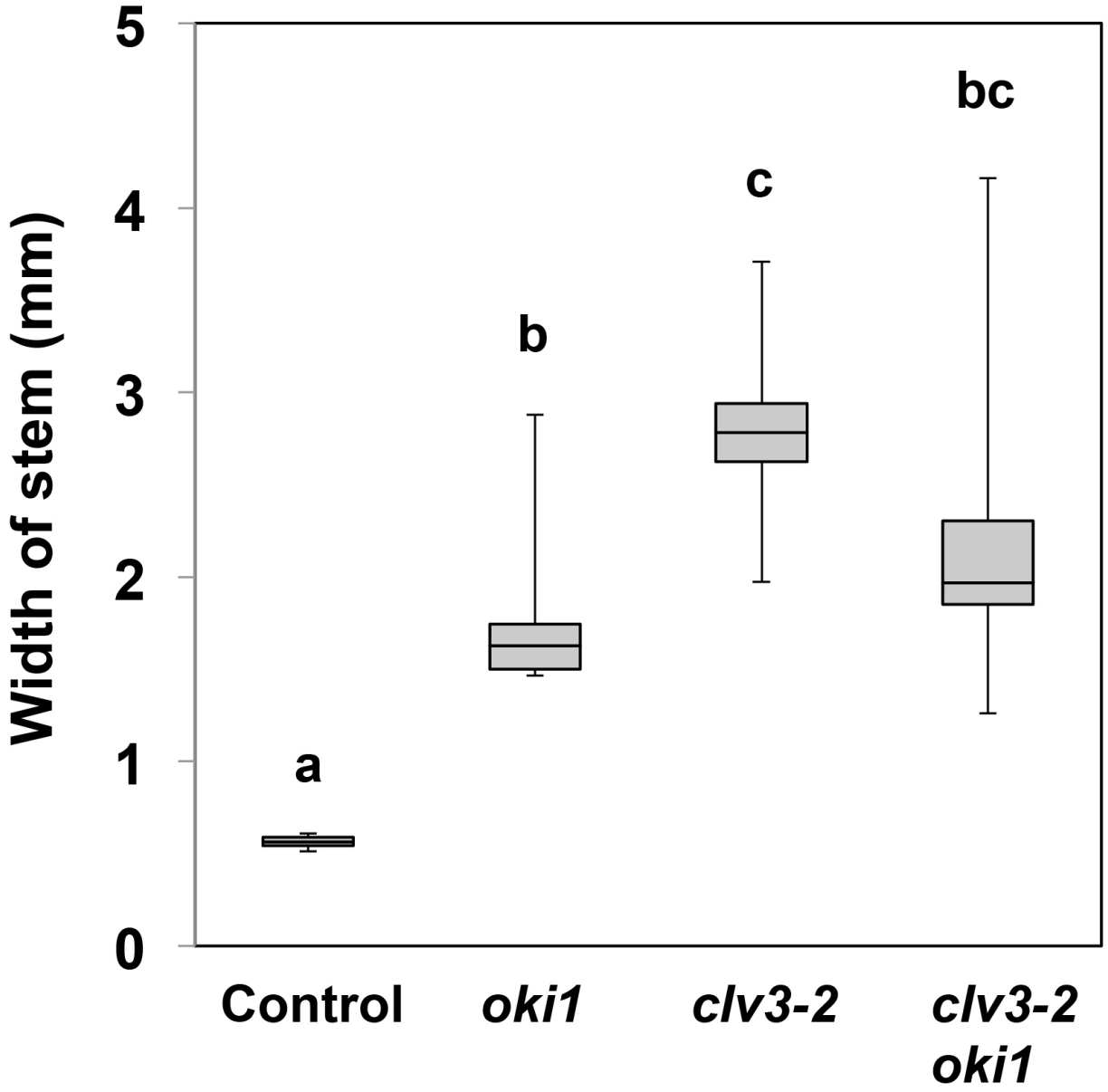

Figure S5. *clv3* is epistatic to *oki1* in stem thickness control. There was no significant difference in stem thickness between *oki1* or *clv3-2* single mutants and *clv3-2 oki1* double mutants, suggesting that *clv3-2* are epistatic to *oki1* in regulation of stem thickness. N = 7-10. Bars topped by different letters are significantly different at $P < 0.01$ (Tukey HSD test).

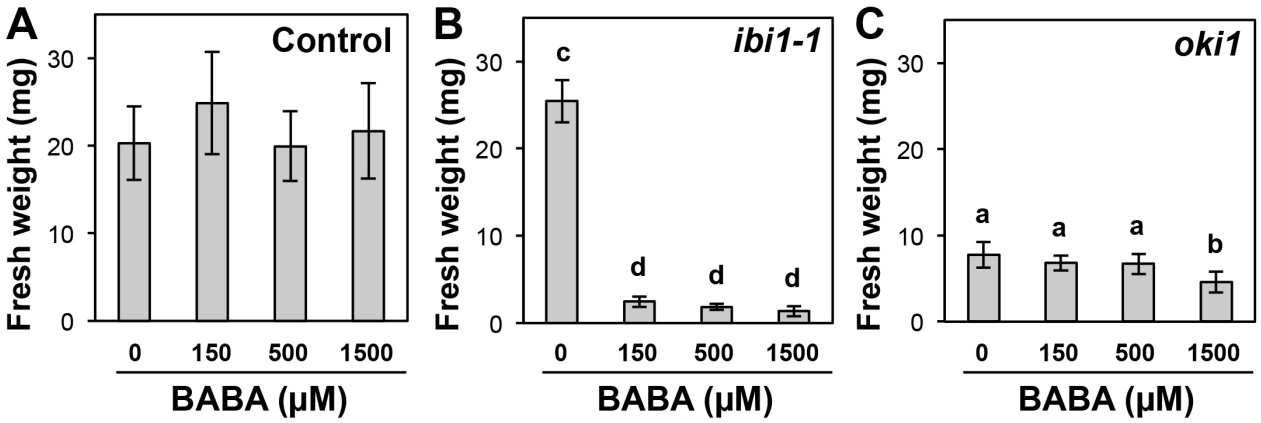

Figure S6. *oki1* mutants are not hypersensitive to BABA. (A, B) 150-1500 µM BABA did not affect to the growth of control line (A), but significantly inhibited the growth of *ibi1-1* mutants (B), as expected. (C) 150-500 µM BABA did not affect to the growth of *oki1* mutants, although it was decreased in presence of 1500 µM BABA. N = 8-10. Bars topped by different letters are significantly different at $P < 0.01$ (Tukey HSD test).

Table S1. Oligonucleotides used as primers in this study.

Primer sets for genotyping.			
Mutants	Forward	Reverse	Note
oki1	GAGCTATGCGGCGAGTTATC	GAAAGTTCATTGCTGAGACGAA	PCR product was digested with HpaII. WT: 116bp / 113 bp, *oki1*: 229 bp.
wus	GGTCTTGCGAAGGATAGTGG	TTGCCCATCCTCCACCTACG	
clv3-2	CTCACTCAAGCTCATGCTCACG	GGGAGCTGAAAGTTGTTTCTTGG	Muller et al., 2008
SAIL_358_B08	CCTTATGATGCAGGCGAGAT	GCTGGCACTCTGAACAACAA	PCRs were performed with LBb1.3 primer (http://signal.salk.edu/tdnaprimers.2.html)

Primers for construction.	
Primer #	Sequence
1	CCTCGGAAGTCGATCCAAAGCAGCTTCAAGATCTCTCCATCCGCACCAAAGGAGGTGGAGGTGGAGCT
2	TGATGTTAAGAGTAAACAGAAGATACAATTGTTTGTGTTGAGAGCTATTAGGCCCCAGCGGCCGCAGCAGCACC
3	GTCTTGATCTGCGCCGTCAGCAAATGAAGAATAATATAGTTCTTCGCCATGGAGGTGGAGGTGGAGCT
4	TTCAAATAGAGTAGGAACACACCTCAATAAAACCATGTCTGTCTTCTAGGGGCCCCAGCGGCCGCAGCAGCACC
5	AAGATTGGTCAAGCATGGTTG
6	TGTCAAAAGTGGGAATTTTGC
7	GGTAGTTGCAGAGCATGTTG
8	CCTGAATTCTTGACGGAACCAG